Future navigability of Arctic sea routes:

High-resolution projections of the Arctic Ocean and Sea Ice decline

Yevgeny Aksenov[1], Ekaterina Popova[1], Andrew Yool[1], A.J. George Nurser[1], Timothy Williams[2], Laurent Bertino[2] and Jon Bergh[2]

(1) National Oceanography Centre, Southampton, SO14 3ZH, UK

(2) Nansen Environmental and Remote Sensing Center, Bergen, N-5006, Norway

Email: yka@noc.ac.uk (corresponding author, Tel: +44-2380-599582)

ekp@noc.ac.uk

axy@noc.ac.uk

agn@noc.ac.uk

timothy.williams@nersc.no

laurent.bertino@nersc.no

jon.bergh@nersc.no

Abstract

The rapid Arctic summer sea ice reduction in the last decade has lead to debates in the maritime industries whether one could expect an increase in cargo transportation in the region. After a dramatic drop in Arctic maritime transport in the 1990s and 2000s, the number of vessels sailing along the Northern Sea Route (NSR) increased from 4 in 2010 to 71 in 2013, before declining to 53 in 2014. Shipping data shows a reduction in average sailing time from of ca. 20 days in 1990s to 11 days in 2012-2013, attributed to easing sea ice conditions along the Siberian coast. However, the economic risk of exploiting the Arctic routes is substantial. It lies in the uncertainty of the length of the navigation season, and in changes in sea ice and ocean, and requires robust environmental predictions. Here a detailed high-resolution future projection of ocean and sea ice forced with the RCP8.5 IPCC emission scenario is used to examine navigability of the Arctic sea routes. In summer, opening of large areas of the Arctic Ocean previously covered by pack ice to the wind and surface waves leads to the Arctic pack ice cover evolving into the Marginal Ice Zone (MIZ). In winter, Arctic sea ice extent decreases to 14.8 million km^2 in the 2030s and to 8.8 million km^2 by the end of the 21^{st} century. Using the projected sea ice and ocean model data and the Arctic Transport Accessibility Model, the summer season sailing times along the Arctic North Pole Route (NPR) in the mid 21^{st} century are estimated to be of 13-17 days, which makes the this route as fast as the NSR. The new emerging state of the Arctic Ocean features large areas of ice-free ocean, fragmented and thinner sea ice, stronger winds, ocean currents and waves. It presents new challenges for resources mining and transportation in the Arctic and for forecasting.

Keywords: Arctic Ocean, shipping, CO_2 emission scenarios, climate change projections, sea ice, Marginal Ice Zone, ocean waves

1. Introduction

The United Nations Framework Convention on Climate Change (UNFCC) held in Copenhagen in December 2009 agreed that global greenhouse emissions, including shipping, must be capped to prevent global temperature rising by more than 2°C. This places heavy challenges on the industry. The estimated share of CO_2 emissions from shipping in the total global anthropogenic CO_2 emissions was about 3.3 percent in the 2000s [1]. Taking into account the projected increase in the volume of shipping, the emissions from global shipping operations will rise by 20-60 percent by 2050. To achieve the target global CO_2 concentration level of 450 ppm by 2050, global shipping is targeted to reduce its emissions at the rate of 2.6 percent/yr from 2020 to 2050 [2-4]. The measures put in place by the International Maritime Organisation (IMO) [5,6], including the recently adopted Energy Efficiency Design Index (EEDI), do not guarantee reaching the required reduction. Additional solutions must be sought, like switching to low-emission fuels, such as Liquid Natural Gas (LNG), hydrogen, biofuels, or non-emissive propulsion, solar- and wind-powered [7], reducing the water drag of ship's hulls and reducing the speed of sailing for cargo vessels (slow steaming). These measures will require several years to implement, and will require refitting the existing fleet at a very large expense for industry [8,9].

The exploitation of shipping routes in the Arctic Ocean can, in principle, reduce the navigational distances between Europe and Asia by about 40 percent, saving fuel and reducing CO_2 emissions [10]. Schøyen and Bråthen analysed a potential reduction in sailing time, fuel and CO_2 emission savings for two types of bulk cargo vessels sailing along the Northern Sea Route (NSR) instead of via the Suez Canal [10]. They concluded that the main advantage of shipping operations using an ice-free NSR would the reduction of sailing time, more then doubling of the fuel efficiency and reduction of CO_2 emission (49-78 percent

emission savings), however asserting that this would not necessary be the case for liner shipping, as an uncertainty in schedule reliability on the NSR is a principal obstacle and, in the short term, this route would first be of an interest for bulk shipping. Overall, the saving in fuel, might not necessarily translate to cost savings because of other factors, such as, higher building costs for ice-classed ships, non-regularity and slower speeds, navigation difficulties, greater safety risks, etc., and, probably the most important factor, fees for icebreaker services. [10,11].

Here it is important to distinguish between trans-Arctic navigation, i.e., transporting cargo between Europe and Asia (and vice versa), which is driven by reducing navigational distances, and the regional Arctic shipping of commodities to Arctic settlements and natural resources from the Arctic. The present study addresses the former, whereas the latter has somewhat different economic controls (such as the quantity and type of cargo, commodity prices, vessels draft and accessibility of the few existing ports along the Arctic routes) and as well as social motivation (some of the Arctic settlements are not accessible by roads and can be supplied only by sea [12]. This regional Arctic shipping is beyond the scope of this study. The next section discusses the current state of the Arctic shipping and formulates the aims of the present study.

1.1 Current State of shipping on the Northern Sea Route

Sailing routes between Europe and East Asian ports through the Arctic Ocean along the Northern Sea Route (NSR) are about 6000 nautical miles (1 nm=1,852 m) shorter (43 percent shorter) than the routes around the Cape of Good Hope and are about 2700 nm shorter (25 percent shorter) than the Europe to East Asia routes via Suez Canal (Table 1 in [13]). The NSR route is also shorter than the Panama Canal route by about 5380 nm (e.g., [10]. The use of the shipping route across the Arctic to bring cargo from Europe to Asia and vice versa has

been explored in the 1990s in a series of international projects [14]. Based on Arctic sea ice and other environmental conditions characteristic of the pre-2000s, the International Northern Sea Route Program (INSROP) estimated that the Arctic shipping route along the NSR could save about 10 days of sailing (a reduction of about 50 percent) for general type cargo vessels, compared to the shipping route from Asia to Europe via the Suez Canal. The project concluded that savings in sailing time could be achieved if low ice or ice-free conditions are present along the NSR, although no comprehensive comparison between these two routes was made by the INSROP at that time [15-18]. Schøyen and Bråthen estimated that the NSR reduces the sailing time between Yokohama and London by 44 percent, as compared to the route via the Suez Canal, if the same average speed is maintained on these two routes [10]. These estimates were later put to the test by practice. For instance, in 2012 a Hong-Kong registered general cargo ship "Yong Sheng" of 14,357 tones of gross register tonnage (GRT) sailed between Dalian (China) and Rotterdam (Netherlands) along the NSR [19]. The ship spent 7.4 days on the NSR, at an averaged speed of 14.1 knots (1 knot=1nm per hour) (NSR Information Office, 2015), saving 27 percent of the sailing time by using the NSR, instead of the route via the Suez Canal (35 days vs. 48 days respectively).

The volume of cargo shipping along the NSR reached its peak in 1987 at 6.6 million tons (331 vessels, 1306 voyages), and then declined in 1990s and 2000s almost to zero [20,21] Since the 2000s, the number of cargo-carrying vessels sailing along the NSR has increased to 71 in 2013, with shipped cargo reaching 1.4 million tons. In 2014 there was a drop in the number of vessels sailing along the NSR to 53. Amongst these, 31 vessels transited across NSR and 22 vessels were involved in regional supply operations [22]. Data on the volume of cargo in 2014 are not yet available [22].

The shipping data shows a reduction of sailing time along the NSR from 20 days in 1990s to 11 days on average in 2012-2013. For this calculation the sailing time data is selected only for

transit voyages between the Pacific ports and Europe from the NSR Information Office database [22]. The sailing time reduction is attributed to the easier summer ice conditions (ice extent and thickness) in the last decade [12,23].

Although the Arctic is projected to become seasonally ice-free by the end of the 21st century [24,25], the beginning and the duration of the ice-free season will be different for each of the three principal shipping routes across the Arctic Ocean from Europe to the Pacific Asia: (i) the route along the Siberian Coast, the NSR (between Murmanks, Russia, and the Cape Dezhnev in Bering Strait); (ii) the Northwest Passage (NWP), the route through the Canadian Arctic Archipelago, which for purpose of the present analysis is combined with the Arctic Bridge (AB) between Canada (Churchill) and Europe; and (iii) the North Pole Route (NPR), which runs from Europe via Fram Strait and across the North Pole to the Bering Strait [13,26,27].

Potential economic and environmental risks in exploiting the NSR lie in the uncertainty of the length of the navigation season, and sudden changes in the oceanic and sea ice regimes in the Arctic [13,28]. One of the risks is shipping accidents involving oil spills and contamination of the Arctic environment. Changes in the Arctic will also have ecological and socio-economic impacts. Adaptation to the changes requires detailed environmental predictions of the sea ice, ocean, atmosphere and ecosystem.

Since the Rossby radius in the Arctic is less than a few kilometres [29], the ocean circulation features (boundary current and eddies) may also have scales a few kilometers or less, so high-resolution eddy-permitting/resolving ocean models must be used to obtain realistic and detailed ocean simulations. Advanced modelling capabilities are required to quantify spatial and temporal variability of the sea ice in the Arctic, and assess scenarios of the future retreat of Arctic sea ice. This study demonstrates the use of high-resolution ocean and sea ice models

for long-term predictions of the future state of the Arctic Ocean, focusing not only on sea ice changes, but also on changes in the ocean circulation, ocean waves and wind. All these are key factors for safe navigation. The aims of the study are two-fold: firstly, to examine the navigability of the Arctic sea routes using a realistic high-resolution detailed future projection of ocean and sea ice conditions, and, secondly, to discuss requirements for sea ice and ocean forecasting models in the changing Arctic.

The paper is structured as follows. The model simulations and analysis methods are described in Section 2. A description of the principal results of the study follows in Section 3 and a more detailed discussion of the findings and directions of the future investigations in Section 4. Section 5 summarizes the study and discusses policy implications, followed by the Glossary and Appendices.

2. Data and Methods

2.1 High-resolution model projections

An eddy-permitting projection of sea ice and ocean state using an Ocean General Circulation Model (OGCM) is used to examine changes in ocean circulation and sea ice cover in the Arctic Ocean in 2000-2099. The model (hereafter, NEMO-ROAM025) is a configuration developed in the Regional Ocean Acidification Modelling project (ROAM) [30]. This is a global high-resolution configuration (nominal horizontal resolution of 1/4° or ca. 28 km, increasing to 9-14 km resolution in the Arctic due to the usage of tri-polar model grid and model grid convergence) of the coupled sea ice-ocean European model NEMO (Nucleus for European Modelling of the Ocean). The oceanic component of the model Ocean Parallelisé (OPA 9.10) is described in detail in [31]. The sea ice component is the Louvain-la-Neuve sea ice model (LIM2) updated with the Elastic-Viscous-Plastic (EVP) rheology (formalism prescribing how sea ice cover deforms under external forces) [32,33] and a sea ice thickness

distribution in model cells (fractional areas of the cell occupied by sea ice of different thicknesses). The model has been used extensively for oceanographic research, operational seasonal ocean and climate forecasts [34] and climate studies [35]. It is used in operational and climate research modes by a number of operational agencies and centers, such as the UK Meteorological Office (UKMO, UK), Mercator-Océan (France), Metéo France (France), the European Center for Medium Range Weather Forecasting (ECMWF, EU) and Environnement Canada (Canada). NEMO is part of the Global Monitoring for Environment and Security (GMES) and is used in the Intergovernmental Panel on Climate Change (IPCC) Assessment Reports (AR) as the ocean model component of the CMCC-CM, CNRM-CM5 and IPSL-CM5A(B)-L(M)R climate models [24].

For the present simulation global NEMO-ROAM025 is forced by output from a simulation of the UKMO Hadley Center Global Environment Earth System Model (HadGEM2-ES), run under IPCC Assessment Report 5 (AR5) Representative Concentration Pathways 8.5 baseline (excluding climate policies in capping emissions) scenario, hereafter RCP8.5 [36]. The HadGEM2-ES simulation spans 1860-2099 and included terrestrial and oceanic carbon cycles, atmospheric chemistry and aerosols [37] and is one of an ensemble of runs performed for the Coupled Model Intercomparison Project 5 (CMIP5) and IPCC AR5 [37,38]. The output frequency of the forcing is monthly for precipitation, which includes rain, snow and runoff, daily for downwelling shortwave and long-wave solar radiation and 6 hourly for the atmospheric boundary layer variables: near surface air temperature, humidity and wind velocities [30]. Turbulent air–sea and air–sea ice fluxes are calculated from the HadGEM2-ES output atmospheric fields using standard bulk formulae for the atmospheric near surface boundary layer [39].

The choice to use the high-radiative forcing scenario RCP8.5 was motivated by recent assessment of the current CO_2 emissions [4,40,41], which placed the present-day emission

trajectory within the 5-95 percent range and above the 15-percent centile of the RCP8.5 (on an estimated carbon budget of 34.8-39.3 Gt CO_2 in 2014). This changes RCP8.5 scenario from being an extreme climate impact scenario into a high-likelihood climate change scenario, unless sustained emission mitigation from the largest emitting countries is put in place [41].

The model was integrated in two stages. First, a coarser resolution version of global NEMO-ROAM1 (global nominal horizontal resolution of 1° or 111 km, resolution in the Arctic is of 36-56 km) was spun up for the period 1860-1974 to obtain a near-present climate state [42]. Next, this state (ocean and sea ice) was used as the initial condition for high-resolution integrations for the period 1975-2099. Sea ice concentration, thickness and drift, along with ocean currents, temperature and salinity, and near surface air temperature (at a 10-m height), latent and sensible heat fluxes between the atmosphere and underlying surface, and 10-m-height winds were output as 5-day mean fields. The output fields were then averaged, to give monthly, seasonal, annual and decadal means. The NEMO-ROAM1 model has the same resolution as the highest resolution of the CMIP5 models (resolution of 1-2°) and its results are largely comparable with those from the CMIP5 ensemble [24,30], whereas the NEMO-ROAM025 has a 4-times higher resolution. Both the NEMO-ROAM configurations have vertical resolution almost twice as in the CMIP5 models (75 levels in NEMO vs. 30-40 levels in the CMIP5 models), with 19 levels in the upper 50 m and 25 levels in the upper 100 m. The thickness of the top model layer is ~1 m and partial steps in the model bottom topography are used to improve the accuracy of the model approximation of the steep continental slopes. The advantage of the high-resolution NEMO-ROAM025 projections, when compared to the CMIP5 ensemble, is in more realistic simulations of the ocean currents in the Arctic Ocean and elsewhere because it resolves most of the ocean eddies while “permitting” small eddies, and improves simulations of the Arctic Ocean Boundary Current, a principal conduit of the

warm Atlantic water in the Arctic Ocean [29,43]. The high vertical resolution and partial bottom steps also improve simulations of the ocean currents on the continental shelf, which is essential for modeling surface ocean dynamics and sea ice. The model has a non-linear ocean free surface, improving simulations of the sea surface height and changes in sea level. For detailed discussion of the model setup please see [42].

The present study also uses the lower resolution projection of NEMO-ROAM1 forced with the same RCP8.5 HadGEM2-ES output described above, and with the IPCC AR5 RCP2.6 low emission stabilisation scenario [40,41]; both simulations have run continuously for the period 1860-2099 [30]. The integrations were used to examine changes in the sea ice and ocean under different emission scenarios.

2.2 Ship safe speed and Sailing Times

The approach taken here is to utilize the high-resolution projection described above to provide a quantitative assessment of Arctic accessibility for shipping in the 21st century. In the present study the Arctic Transport Accessibility Model (ATAM) [12,44] is applied to the sea ice fields from the projections with NEMO-ROAM025 to calculate safe ship speed (SS) and sailing time (ST) along the Arctic routes. The method closely follows the papers of [12,44], which is the first published use of ATAM. The ATAM model assumes sea ice conditions are the primary factor impacting the SS and ST in the Arctic Ocean and employs a concept of Ice Numerals (IN) developed by the Arctic Ice Regime Shipping System (AIRSS) [45] in determining ships' ability to navigate sea-ice-covered ocean (eqn. 1, Appendix 1). The AIRSS algorithm defines IN as a sum of Ice Multipliers (IM) for different ice types weighted by their partial fraction. Ice types are derived from the stage of ice development (sea ice age, Table 1, Appendix 1), which, following [12,44] are defined from ice thickness [46]. IM are obtained empirically according to different ship classes, taking into account ice types [45]. If IN is

positive, the ice conditions are unlikely to be hazardous, thus navigation is safe and SS can be calculated and sailing times along the chosen route are obtained (eqn. 2, Appendix 1). If IN is zero or negative, the ice conditions may be dangerous and sailing unsafe and SS is set to zero (Table 2, Appendix 1). It should be noted, however, that the IN should be considered only as guidance, and the ultimate decision whether to proceed lies with the ship's Master [45].

A major simplification in the IM calculations made in this study, as well as in previous studies [12,21,27,44] is that IM depends only on ship classes, concentration of different sea ice types and sea ice thickness, but does not explicitly account for ice roughness (area of ridged ice) and ice decay parameters. The reason for this is that thermal ice decay is not routinely available in sea ice models and has been only recently included in the Los-Alamos CICE sea ice model as an extra prognostic variable [47], and ice roughness is not always included in current sea-ice models. The absence of these parameters from sea-ice models is partly due to the lack of robust observational remotely-sensed data that might be used to validate and be assimilated into the sea-ice models, and currently these sea ice parameters are still derived qualitatively from visual observations [44,48].

Summer navigation (defined as from June to October, JJASO) conditions along the NPR in the 21st century are assessed for the following 7 types of cargo vessels currently sailing in the Arctic: Canadian Arctic Categories CAC3 (Polar Class 3, PC3) and CAC4 ice-capable vessels and general cargo vessels Types A-E. Type A corresponds to moderately ice-strengthened Polar Class 6 (PC6) and Type E is non-ice strengthened open water vessel (OW) [12,26,45,49]. The ATAM model is used with monthly mean sea ice thicknesses and concentration fields for the decades 2010-2019 (near future state of the Arctic) and 2030-2039 (medium-term state of the Arctic). The results along the NPR are compared with the SS and ST for the three Arctic routes (NSR, NWP-AB and NPR), as assessed by [12,26]. Since in NEMO-ROAM025 with RCP8.5 forcing the summer Arctic sea ice is very low after the

2050s, a different approach, detailed in the next section, is explored to examine conditions in the Arctic over this period.

2.3 Sea Ice Fragmentation and Waves in Marginal Ice Zone

The definition of the Marginal Ice Zone (MIZ) varies between different publications. The approach taken in this study is based on satellite products and considers sea ice covered areas with concentration 0.15-0.80 as MIZ [50].

Information on sea ice cover fragmentation (the two-dimensional distribution of maximum ice floe sizes) is presently not routinely available from forecasts or satellite products. For the MIZ in the Arctic the distribution of maximum ice floe sizes can be parameterized following [51] as an exponential function of the sea ice concentration (eqns., 2–3, Appendix 2). The limitation of this approach is that the parameterisation has been developed from the analysis of data from Fram Strait, and so may not represent conditions in the compressed winter ice pack. However, with the decline of sea ice and widening of the MIZ in the Arctic, the winter ice pack will occupy less area and this parameterisation should be sufficiently accurate for the present analysis. Since the NEMO-ROAM025 projection does not include ocean waves, a quadratic dependency of significant wave height H_w on wind speed U_{wind} is assumed for simplification: $\frac{H_{w2}}{H_{w1}} = \left(\frac{U_{wind2}}{U_{wind1}}\right)^2$; indices 1 and 2 refer to wind speed and wave heights at times 1 and 2. This allows us to obtain an estimate of the H_w increase, although this does not account for the wave fetch increase [52]. For the short-term forecasting the coupled wave and sea-ice models can be used as is it shown in the Section 3.5 [53].

3. Results

3.1 Verification of the Sea Ice Model

To evaluate the model skills and biases in simulating present Arctic sea ice cover, simulated spatial distribution of sea ice concentration (fractional area of the ocean covered by ice) along with time series of the pan-Arctic sea ice extent (the area over which ice is present) and volume (product of ice thickness and concentration) are compared with observational datasets and reanalyses. This model evaluation guides the assessment of the projected future sea ice and ocean state.

Observed sea ice concentrations are taken from the UKMO Hadley Centre Sea Ice and Sea Surface Temperature (HadISST1) dataset [54]. The HadISST1 dataset is based on the multidecadal passive microwave satellite remote sensing products of the global sea ice cover from 1978 until present (hereafter 2014). In order to examine model performance in different seasons, monthly simulated and observed sea ice concentration fields are averaged for winter (December-February, DJF), spring (Mar-May, MAM); summer (June-August, JJA) and autumn (September-November, SON) for 1978-present, thus creating mean seasonal averages for this period.

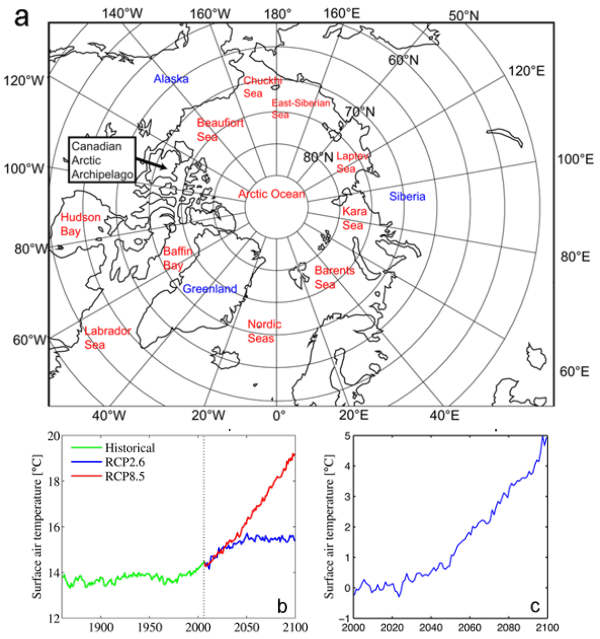

Fig. 1. (a) Region of the study. (b) Timeseries of the global annual mean surface air temperature 1860-2099 in the RCP2.6 and RCP8.5 projected atmospheric forcing and (c) of the pan-Arctic annual mean surface air temperature 2000-2099 in the RCP8.5 forcing.

The realism of the simulated variability and trends in sea ice are assessed by comparing monthly timeseries of sea ice extent obtained from HadISST1 with those from the model and by comparing simulated sea ice volumes with those from the Pan-Arctic Ice-Ocean Modeling and Assimilation System reanalysis (PIOMAS) [55]. The sea ice extent time series is computed by summing two-dimensional monthly sea ice extent fields for 1978-2013 over the area north of 65°N, including the Arctic Ocean, the Arctic shelf seas and the waters of the Canadian Arctic Archipelago, the Nordic Seas, the Baffin Bay, but excluding the Hudson Strait and Bay, the Labrador and Bering seas (Fig. 1a). The simulated volumes are integrated over the area above for 1979-2005 and compared to those from the PIOMAS.

The sea ice state for the current climate (1970s–2010s) simulated by NEMO-ROAM025 agrees with data (Fig. 2 and 3). Winter ice fractional concentration (or ice fraction) in the model and data is in good agreement (Fig. 2a,c). In the model there is a moderate underestimation of summer sea ice fraction north-east of Svalbard and an overestimation of ice summer fraction the Chukchi and East Siberian seas (Fig. 2b, d). The simulated sea ice extent and volume trends are consistent with that currently observed (Fig. 3a,b,c), although the model overestimates both sea ice extent by about 7 percent and 15 percent in the winter in the summer respectively (Fig. 3a,b) and annual volume by about 15 percent (Fig. 3c,d).

3.2 Changes in Sea Ice

The NEMO-ROAM025 high-resolution forward projection, forced with the RCP8.5 scenario, and the lower-resolution NEMO-ROAM1 forced by both RCP8.5 and RCP2.6 forcing give a consistent picture of sea ice changes in the 21st century, as compared to the CMIP5 model scenarios (Fig. 3e,f) [24,37]. Both NEMO-ROAM simulations and the corresponding IPCC AR5 RCP8.5 models appear similarly too conservative in predicting currently observed sea ice decline (sea ice reduction in the models is too low) [56-59]. Moreover, there is a little difference in both, the sea ice extent and volume between the NEMO-ROAM025 and

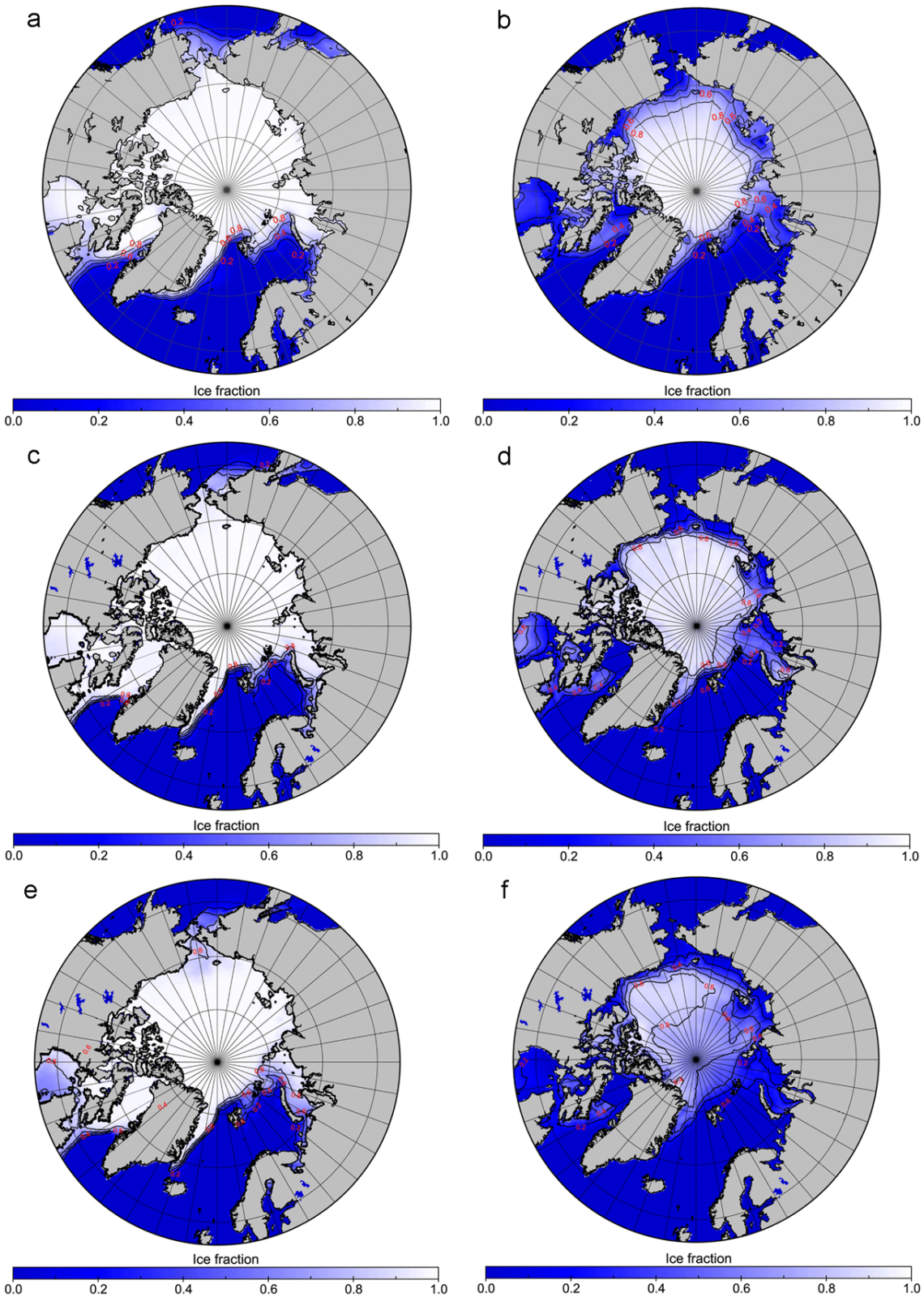

Fig. 2. (a,c,e) Mean 1978-2005 winter (Dec–Feb) and (b,d,f) summer (Jun–Aug) sea ice fraction (color and black contours) from the HadISST1 [54] (a, b) and from the NEMO-ROAM025 model (c, d). (e) Model winter (Dec–Feb) and (f) summer (Jun–Aug) 2030–2039 ice fraction from the NEMO-ROAM025 RCP8.5 projection (color and black contours).

NEMO-ROAM1 forced forward projections on one hand, and the respective HadGEM2-ES coupled simulations on the other (cf., Fig. 3a,b,c and Fig. 3 and 4 in [60]). Since, the forced and coupled models show a similar sea ice response to the warming, the conservative biases in the projections are not due to the lack of ocean-ice-atmosphere feedbacks, but because of deficiencies in the physical description of the underlying sea ice processes [57,59]. Until the 2050s NEMO ROAM projections closely follow the CMIP5 RCP8.5 ensemble mean and for the 2060s-2090s are within 5-95 percent of the CMIP5 ensemble (Fig. 3e,f).

The RCP8.5 scenario presents a substantial increase in global and Arctic surface air temperatures (SAT) (Fig. 1b,c) and in Arctic sea surface temperature (SST). Between the 2000s and 2090s, SST in the Arctic Ocean and Siberian seas increases by about 2°C in the winter and by about 7°C in the summer, reaching averaged values of about 2-3°C and 5-8°C in the winter and summer respectively (not shown). Similar to the CMIP5 RCP8.5 model ensemble, the model presents conservative simulations for the current sea ice climate (Fig. 3e,f). The NEMO-ROAM1 sea ice simulations with RCP8.5 are similar to those with NEMO-ROAM025, except for the last ten years of the integrations, when ice in NEMO-ROAM025 declines more slowly than in NEMO-ROAM1 in the winter and more rapidly in the summer.

In both runs the shape of the volume seasonal cycle does not change with declining ice, although there is a clear reduction in the mean and the amplitude of the cycle. The seasonal cycle of mean ice thickness changes: the maximum shifts from June to May and the secondary maximum in September, due to melting of first-year ice, disappears (Fig. 3d). In the model projection, summer ice retreats first in the Eurasian Arctic and in the Siberian seas (Fig. 2) but there are only moderate changes in winter ice extent until the 2030s, from 16.2 million km^2 in 2000-2009 to 14.8 million km^2 in 2030-2039 (area changed from 15.4 million km^2 to 14.1 million km^2) (Fig. 3a,b). Ice retreats more rapidly from the 2030s with ice extent reaching 8.8 million km^2 (area of 7.7 million km^2) in the Arctic by the 2090s (Fig. 3a,b).

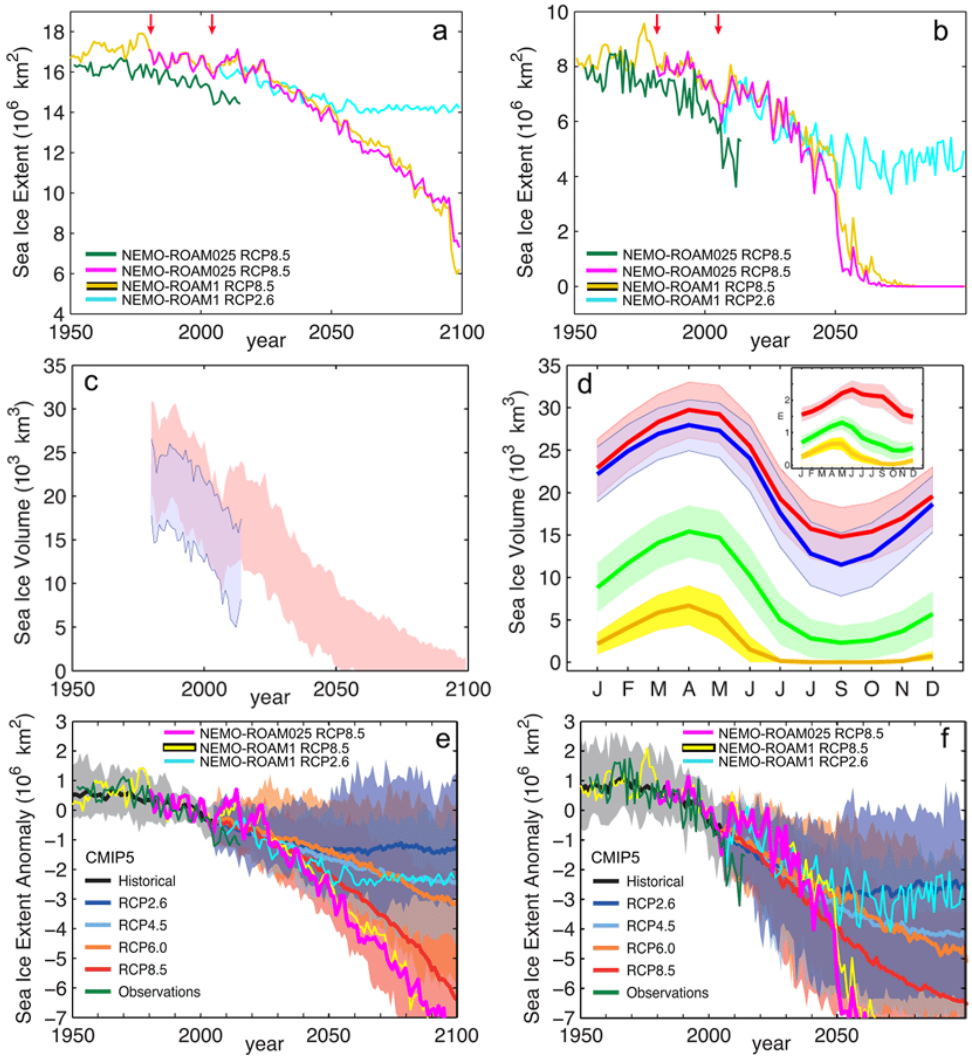

Fig. 3. (a) winter (February) and (b) summer (September) observed sea ice extent 1953–2015 (green line) from NSIDC [61] and HadISST[54] datasets and simulated 1953–2099 in NEMO-ROAM025 RCP8.5 (magenta), NEMO-ROAM1 RCP8.5 (yellow) and in NEMO-ROAM1 RCP2.6 simulations (light blue). Red arrows show the start of the NEMO-ROAM025 run in 1978 and the end of the historical forcing and beginning of the projected RCP8/5/2.6 forcing in 2005. (c). Monthly ice volume simulated by NEMO-ROAM025 RCP8.5 (red) and from PIOMAS (blue) for 1980-2015. (d) The corresponding modelled seasonal cycle of ice volume (red) and from PIOMAS (blue). Modelled seasonal volumes are also shown for 2030-2059 (green) and 2060-2099 (yellow). The insert shows the corresponding seasonal cycles of modeled mean ice thicknesses. Solid lines mark means and color shading denotes ±one standard deviation. (e) Winter and (f) summer sea ice extent anomaly (relative to the 1986-2005 winter and summer means respectively) in the NEMO-ROAM025 RCP8.5 simulations (magenta) and in the NEMO-ROAM1 simulations forced by RCP8.5 (yellow) and RCP2.6 (light blue). The corresponding sea ice extent anomalies in the CMIP5 ensembles for the different emission scenarios from the IPCC report [37] are shown as solid color lines with shading denoting 5 to 95 percent of the ensembles. Green lines depict the observed winter and summer sea ice extent anomalies 1953-2015 obtained from NSIDC and HadISST datasets.

3.3 Changes in Ocean Circulation

The oceanic geostrophic balance (i.e., ocean pressure gradient is balanced by the Coriolis force) holds in the Arctic Ocean (except for near surface fresh water-driven flows) for time averaging longer than a month, which permits the ocean circulation to be analyzed using the Montgomery function, mapped on pseudo-neutral surfaces [43].

The method allows the use of scalar stream-function-like surfaces instead of the vector fields, and simplifies analysis of the ocean circulation and attribution of driving mechanisms. The present analysis is focused on the effects of wind on the upper ocean dynamics (down to 600 m depth). To examine the changes in the surface ocean currents two-dimensional fields of sea surface height are analyzed as an approximation of the geostrophic surface circulation.

Like the sea ice, the surface circulation shows a large change after the 2040s. The anti-cyclonic circulation in the Beaufort Sea of the Canadian Basin, a characteristic of the present-day Arctic circulation [62,63], disappears, and a large cyclonic gyre develops in the western Arctic Ocean, with a strong localized anti-cyclonic gyre in the East-Siberian Sea and in the eastern Canadian Basin (Fig. 4a,b). The principal driving mechanism is reduction of the high atmospheric sea level pressure (SLP) in the Beaufort Sea and decrease of the Ekman convergence in the Beaufort Gyre [64]. The other feature is the "short-circuiting" of the Arctic surface circulation in the Nordic Seas, resulting in the Arctic surface waters recirculating back in the Arctic Ocean, instead of flowing out into the North Atlantic (Fig. 4a,b). The Montgomery potential shows a similar change from a weak cyclonic boundary flow at intermediate (200-600m) depths in the Canadian Basin after the 2040s (Fig. 4c,d). This change also results from changes in the atmospheric wind, which increase the high oceanic pressure (high Montgomery potential) in the Central Arctic in the 2090s and block the boundary current emerging northwards from the Barents Sea driven by the high oceanic pressure that is present in the Barents Sea before the 2040s (Fig. 4c,d).

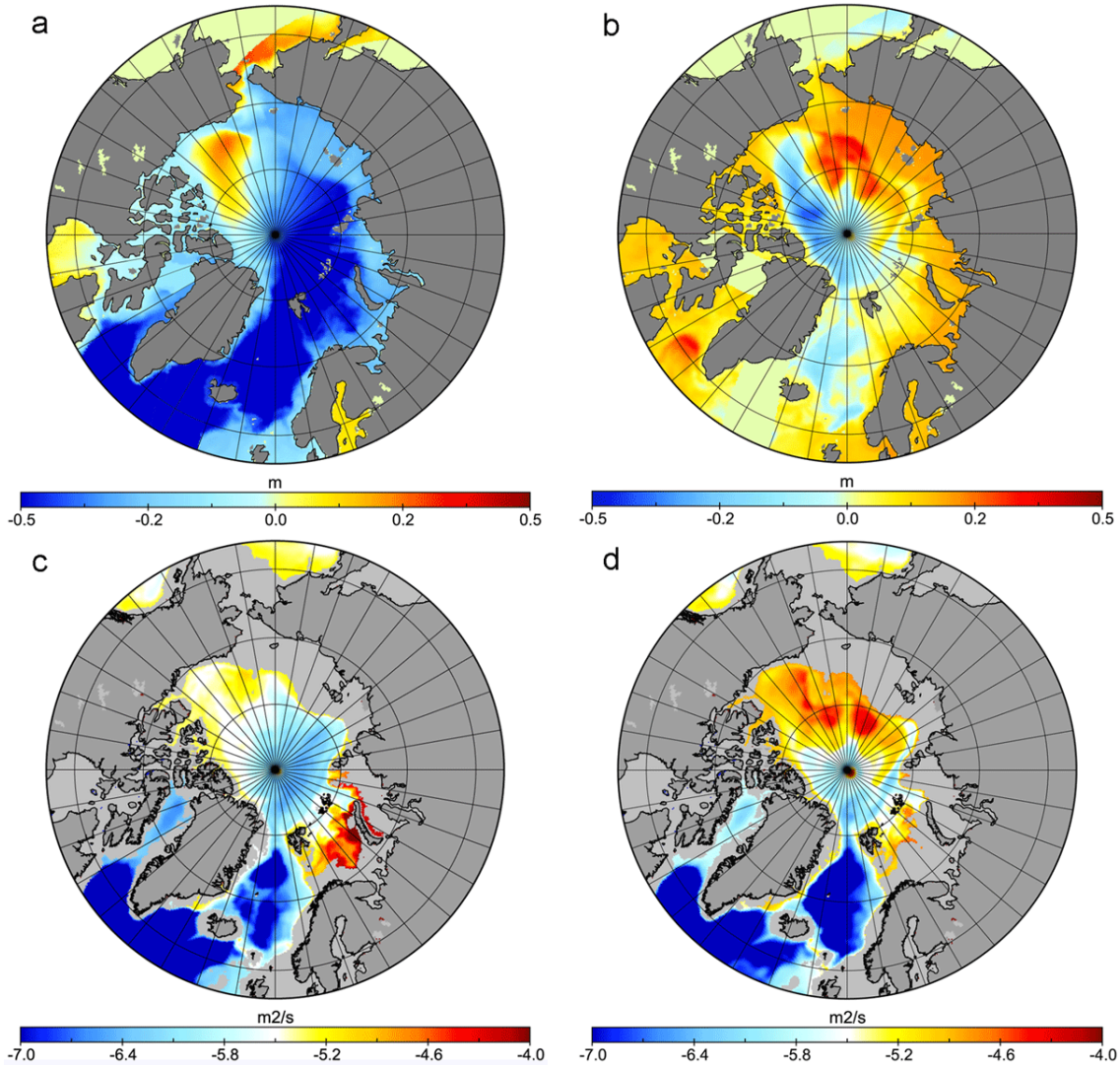

Fig. 4. Model mean sea surface heights (a) in 2040-2049 and (b) change between 2000–2009 and 2090–2099 from RCP8.5 NEMO projection. Mean 2040–2049 (c) and 2090–2099 (d) Montgomery potential (equivalent of geostrophic streamfunctions) at the 27.8 kg/m^3 density surface (about 300-600 m depth) from the same projection.

3.4 Accessibility of Summer Shipping Routes

Following the method described in Section 2.2, the ships safe speed (SS) on the NPR is calculated for the 7 ship classes (CAC3, CAC4, and Types A-E) for the projected averaged summer sea ice conditions in 2010-2019 and 2030-2039. For each model cell Ice Multipliers (IM) and Ice Numerals (IN) are computed (Tables 1 and 2). To obtain the corresponding sailing time (ST) on the NPR, the shortest path in the model domain between Aberdeen (UK) and Bering Strait is defined (Fig. 5). In addition, optimized routes to avoid impassible ice type for each of the 7 ship classes are defined via choosing a path through the 2-D IN fields, which

steps only through the positive IN values and minimizes the distance between the port of departure (Aberdeen, UK) and destination (Bering Strait). All sailing times are calculated by summing up the times required to cross each of the model cells along a selected route.

In the 2010s, the thick and compact second year ice remains in the Central Arctic on the NPR (Fig. 5a) and the route is inaccessible for the Type A-E general cargo vessels, The ice-capable vessels CAC3 (PC3) and CAC4 can navigate the NPR by avoiding areas of thickest ice in the Canadian Basin (Fig. 5a). The sailing time estimates are of 16-20 days for these optimised routes (Table 3). To transit the high Arctic, Type A (PC6) vessels have to avoid multi-year and second year pack ice and thick first-year pack ice as well. This pathway takes these vessels far away from the NPR, almost along the NSR (Fig. 5a). Easier ice conditions on the NSR but longer distances result in the sailing time of 20 days (Table 3). The less ice-capable Type B-E are unable to safely break compact pack ice thicker than 0.7 m, therefore they cannot transit the Arctic Ocean offshore and have to follow the NSR (Fig. 5a). The inaccessibility of the NPR for general cargo vessels until end of the 2010s in the present analysis is consistent with the results by Smith and Stephenson [26], who performed the Arctic shipping accessibility analysis using the CMIP5 ensemble and concluded that the direct route across the North Pole is closed for PC6 (Type A) and open water OW (Type E) ship classes (Fig. 2 in [26]).

During the summers in the 2010s and 2020s sea ice concentration in the Central Arctic is predicted to be in the range of 70-100 percent (the ocean is covered in close pack ice, very close pack ice and compact pack ice [46]) and, therefore, accessibility of the NPR and navigability on the route should be primarily controlled by sea ice thickness (ice types) distribution along the route. To examine this, a series of optimised route scenarios with fixed ice concentration and perturbations in the ice thickness fields are assessed. It should be noted

that all the calculations presented here assume unescorted sailing. If icebreakers support is used, the NPR can be more accessible for the other classes of vessels.

In the 2030s, a large part of the NPR in summer is either ice-free or is covered in open ice (ice concentration of 40-60 percent [46] (Fig. 5b) and the four ship classes, CAC3 and 4 and Types A and B can safely access the route (Table 3). For the optimised routes constructed in a similar way as for the 2010s, all general cargo vessels are able to navigate the NPR (Table 3). With the averaged sailing times from 13 to 17 days, the navigation via the North Pole can compete with coastal routes. The sailing times along the NSR were 11 days on average (range of 8-19 days) for the transit shipping in 2012-13 [21,22] and the estimated projected averaged sailing time is of 11 days for Type A vessels in summer 2045-2059 [12].

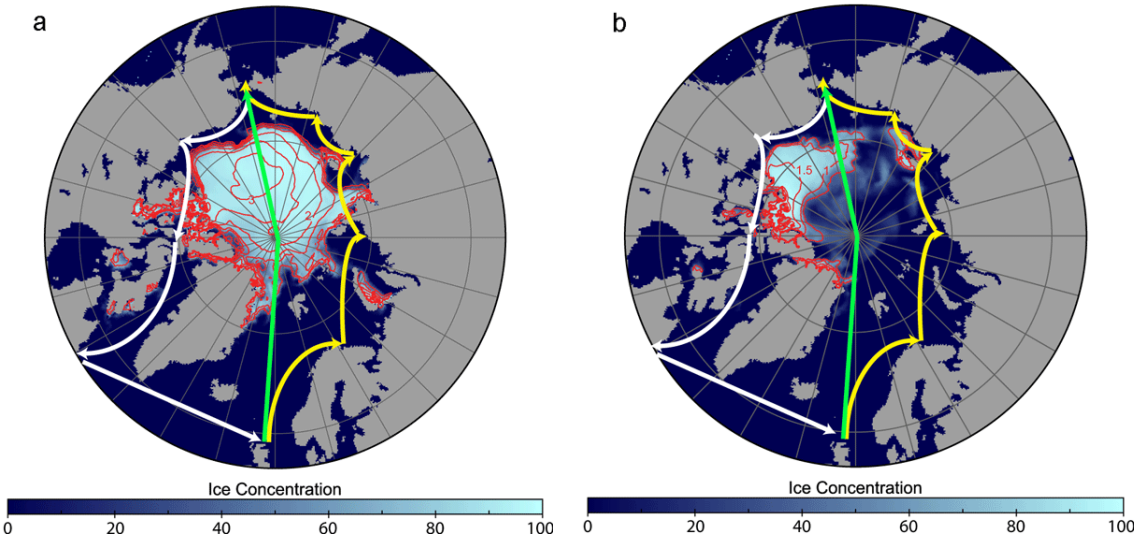

Fig. 5. Model 2010–2019 (a) and 2030–2039 (b) sea ice concentration (percent, color) and thickness (red contours) during the navigation period (Jun-Oct) from the RCP8.5 NEMO projection. The Arctic shipping routes are shown schematically: the Northern Sea Route (NSR) (yellow line), the North Pole Route (NPR) (green line) and the Northwest Passage (NWP) and Arctic Bridge (AB) (white line).

The sailing times along the NPR obtained using the sea ice data from the NEMO-ROAM025 projection agrees well with those obtained using the ATAM with a subset of the CMIP5 models [12,21,27], e.g., average sailing time on the NPR in the 2040-2050s is 16 days for Type A vessels vs. 15 days in the NEMO-ROAM025 analysis (Table 3). This is evident of the

validity of the current approach. The thick sea ice remains in the Canadian Basin in the 2030s and affects navigation along the NWP (Fig. 5), making this route practically non-operational at least until the mid-21st century [12].

After the 2050s, the summer sea ice has a very low extent (less than 1 million km^2) and thickness (less than 0.2 m) (Fig. 3d,f) and does not affect the sailing. All types of examined vessels can safely navigate the NPR. Since, a substantial areas of the ice-covered Arctic Ocean are transformed to MIZ, the main factors affecting the sailing become distances along the route, waves and wind.

3.5 Forecasting in the Marginal Ice Zone

Currently the summer Arctic MIZ is widening, reaching on average about 150 km in width [50] (Fig. 6). The NEMO-ROAM025 projection shows a nearly two-fold increase in the MIZ area in summer between the 1978-2005 and 2030s (Fig. 6a,b and 7e). After the 2030s the MIZ relative area in the summer increases from about 20 percent to about 90 percent in the 2080s-90s (Fig. 7e). The simulated winter MIZ is about 10 percent in the 2000s, decreases until the 2080s and then increases, constituting about 30 percent of the area of the Arctic sea ice in the 2090s (Fig. 7c,d,e). With the summer MIZ area increasing, the pack ice (ice fraction greater than 0.8) area in the summer declines in the simulations and in the 2050s has about the same area as the summer MIZ (Fig. 7c,d,f). The winter pack ice does not change significantly until the 2090s, when it declines to about 70-80 percent of total ice area (Fig. 7d,f). Both the CMIP5 model ensembles and the NEMO-ROAM025 projection predict changes of the winter ice pack concentration in the central Arctic Ocean from 90-100 percent to 70-90 percent by the 2090s (Fig. 7a,b), caused by erosion of the Arctic halocline in summer, making the heat from the Atlantic and Pacific inflows available to melt ice in winter. This is especially

noticeable in the Barents Sea and Chukchi and Beaufort seas, where the winter MIZ occupies a significant area (Fig. 7a,b,d).

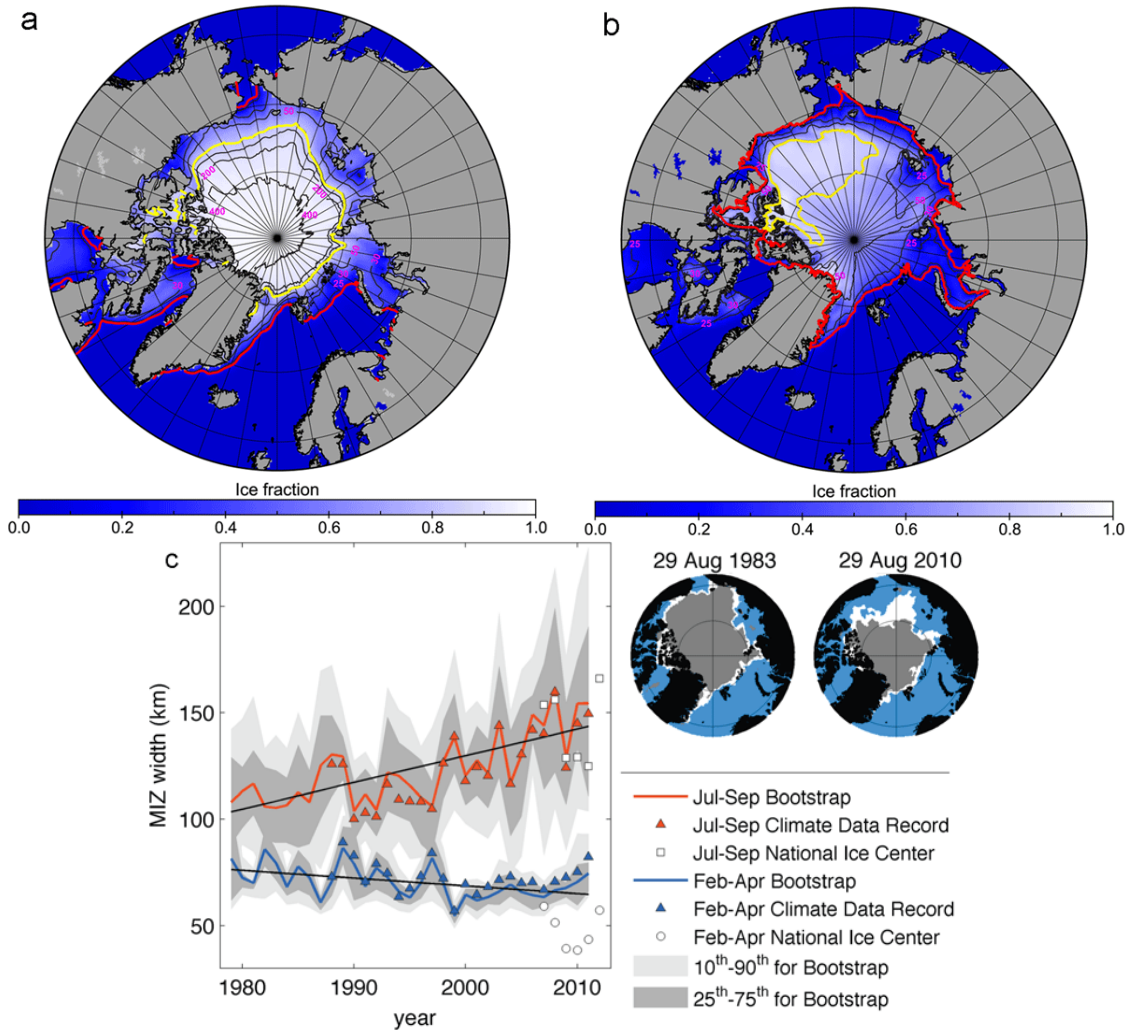

Fig. 6. (a) Mean 1978-2005 summer sea ice fraction (color) and mean floe sizes in metres (black contours with pink labels). Ice fraction is from the Hadley Centre dataset [54]. Red and yellow lines mark the outer (ice fraction of 0.15) and inner (ice fraction of 0.80) boundaries of the MIZ [50]. (b) The same but for 2030–2039 from the NEMO projection. (c) Timeseries 1979–2011 of MIZ width in summer (red) and winter (blue) from [50]; insert shows the MIZ expansion between Aug 1983 and Aug 2010.

Strong and Rigor observed two distinctive tendencies in the summer and winter MIZ width trends during 1978-2011: 39 percent MIZ widening in summer and 15 percent narrowing in winter, and explained the winter MIZ decrease by the thermal impact of the North Atlantic water inflow [50]. Although Strong and Rigor examined MIZ width rather than area, their results are qualitatively compatible with the MIZ area change in the NEMO-ROAM025 simulation for the same period (Fig. 6c and 7e).

In this emerging state of the Arctic Ocean, when open sea ice cover conditions dominate, sea ice fragmentation (floe sizes), wind and waves become the prevailing factors affecting Arctic navigation (e.g., EU Project "Ships and Waves Reaching Polar Regions", http://swarp.nersc.no/). The RCP8.5 forcing demonstrates an increase in winter (DJF) wind speed in the Arctic Ocean by about 50 percent on average (Fig. 8a,b).

Fig. 8c,d shows that this is accompanied by an increase in significant wave heights in the Arctic Ocean by about 100 percent on average. (See Section 2.5 for the calculation method). The ice becomes more fragmented, with the maximum floe size in the Arctic Ocean decreasing from about 100-1000m to less than 50m in the 2030s, whereas the floe size in the MIZ decreases to less than 25 m (Fig. 6a,b). With Arctic sea ice shrinking and becoming thinner, the influence of surface waves is stronger. Consequently, a larger part of the sea ice cover acquires dynamic and thermodynamic properties resembling those in the MIZ, rather than the pack ice (Fig. 6 and 7a,b). These changes require revised approaches to improve the skills of operational simulations and forecasts. Specifically sea ice break-up by the ocean waves and dynamics of the highly fragmented sea ice floes needs to be included in operational modeling [53].

The above approach is taken by the operational modeling and forecasting system TOPAZ (Towards an Operational Prediction system for the North Atlantic European coastal Zones, http://topaz.nersc.no/, [65]. A waves-in-ice module (WIM), which describes propagation and attenuation of waves into ice-covered areas and mechanical breaking of sea ice floes is implemented in the system [53,66,67]. TOPAZ runs experimental forecasts for the North Atlantic and Arctic Ocean at 11-16-km resolution. The system also has a data assimilation component based on the Ensemble Kalman Filter [65]. To study the impact of surface waves during the August 2012 event of strongly enhanced melting in the Arctic Ocean, the WIM has been used in a two week long experiment. A strong low-pressure system builds up over a few

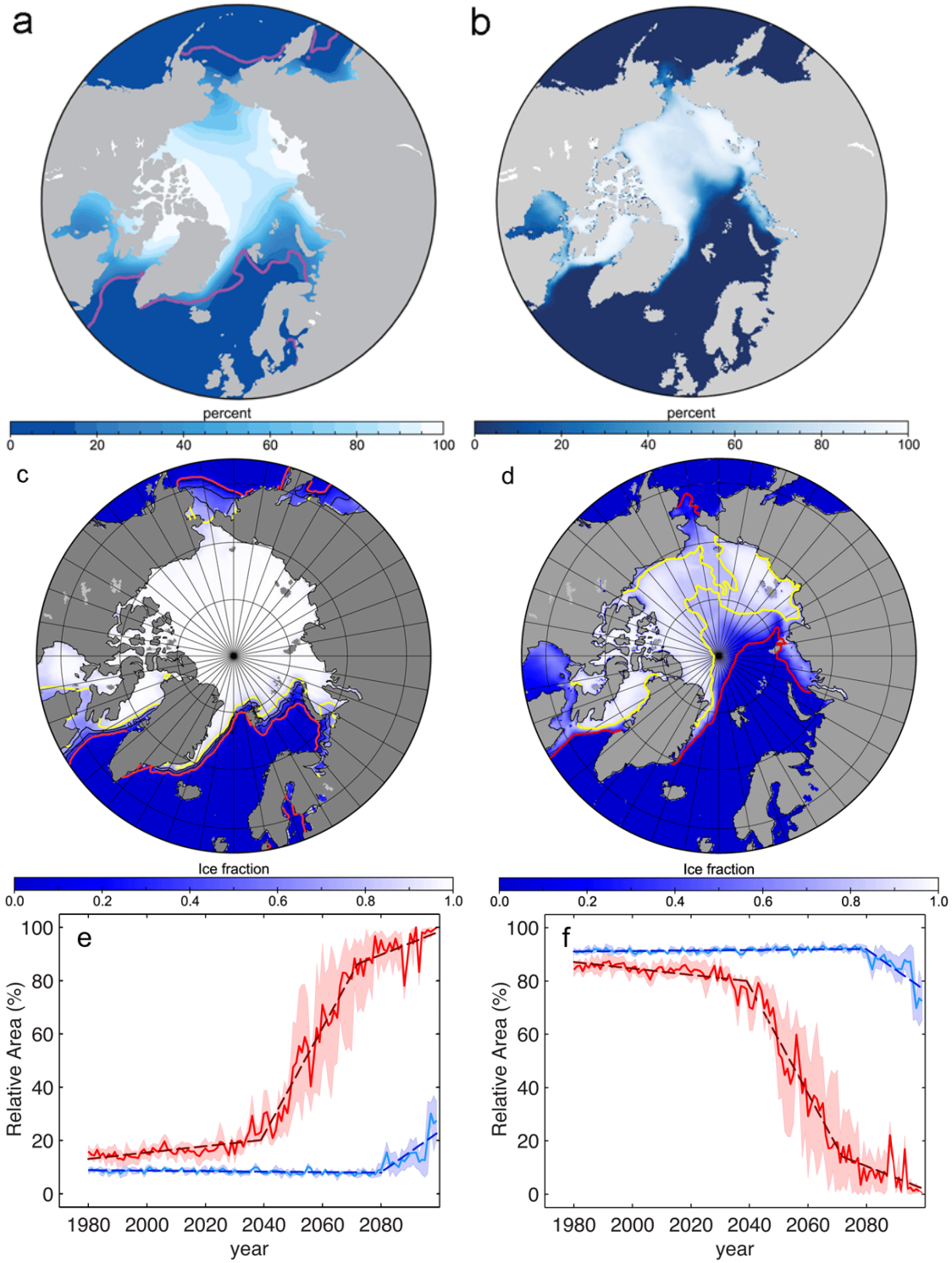

Fig. 7. (a) Ensemble mean winter 2080–2099 ice concentration (percent) in the CMIP5 models with the RCP8.5 forcing (adapted from [37]) and (b) in the NEMO-ROAM025 projection. Please note different colour scales. Magenta line in shows observed 15 percent concentration. (c) Mean 2000–2009 winter sea ice fraction (color) from the HadISST1 [54]. (d) Is the same as (b) but in different colour scale for comparison. Red and yellow lines in (c,d) mark the outer and inner MIZ boundaries. Monthly mean (solid) relative area (percent) of MIZ (sea ice concentration between 15 and 80 percent) (e) and (f) of pack ice (sea ice concentration greater than 80 percent) in winter and summer from the NEMO-ROAM025 projection. The shading denotes ± one standard deviation and dashed lines depict fitted linear trends.

days and generates high amplitude surface waves that are able to travel into the ice-cover and break up the ice into smaller floes (Fig. 9). For instance, the area of broken ice is comparatively larger on the Pacific side of the Arctic where the storms have generated strong waves.

4. Discussion

Several studies have suggested that an Arctic annual surface air temperature increase of ca. 2-3°C has been observed during the last three decades between 1971-2000 and 2001-2012, with the trends about twice higher than those from the RCP8.5 scenario [68,69]. Therefore, it appears possible that the current emissions in the future may lead to even higher Arctic temperatures than climate model simulations with the RCP8.5 emission scenario predict. This could result in faster sea ice decline in the Arctic, than present day climate scenarios suggest, with summer Arctic sea ice disappearance before 2040s [70]. Moreover, with present perennial sea ice reduction to about 20 percent, the Arctic Ocean has become more vulnerable to a potentially rapid transition toward a seasonally ice-free Arctic state, triggered by natural climate variability [71]. The implications of the rapid Arctic state change for the economies of the Arctic regions are anticipated to be substantial. Along with other industries, the Arctic transport system and maritime industries will have to evolve on the short time scale to adapt to the change and mitigate potential consequences [12,44]. The analysis presented in this study suggests that the unescorted navigation in the high Arctic in the summer is possible as early as the 2030-2040s and is probable after the 2050s. The winter seasonal ice in the Arctic will be more fragmented than at present, and its mean thickness will be greatly reduced to about 1 m in the mid 21st century and to about 0.5m in the second half of the century (Fig. 3d). The winter navigation in the high Arctic most likely will still require support from icebreakers due to highly variable sea ice and ocean conditions in this season.

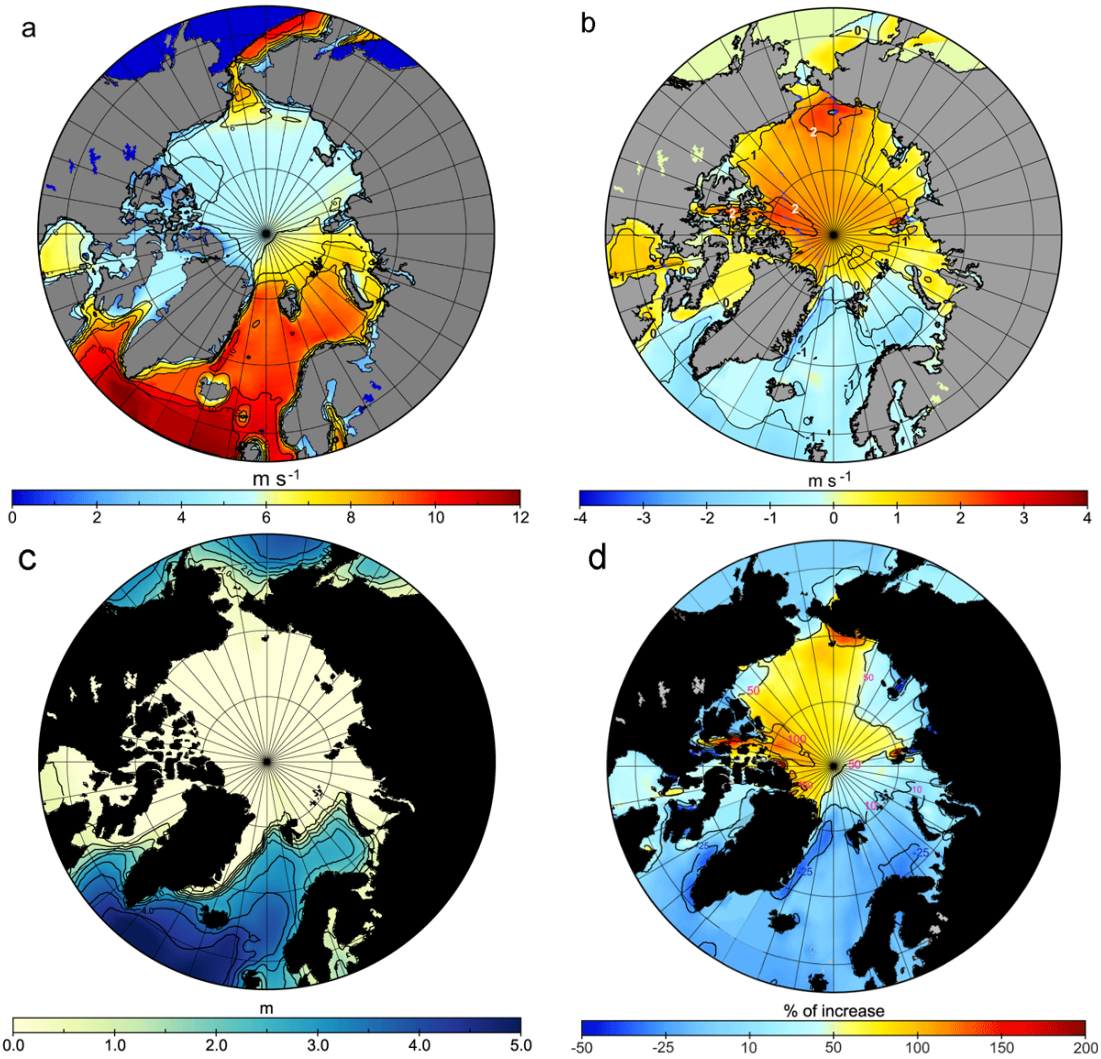

Fig. 8. (a) Mean 2000–2009 10-m height mean wind speed over the ocean and (b) corresponding wind speed change between 2000–2009 and 2090–2099 from the RCP8.5 forcing. (c) Mean 2000–2009 winter significant wave heights (color) from the ECMWF wave model WAM (courtesy Jean Bidlot, ECMWF). (d) Mean 2090–2099 winter significant wave height increase in percent (color and contours) estimated from 10-m height wind speed change between 2000-2009 and 2090-2099 in the RCP8.5 projection.

Stroeve and co-authors analysed sea ice thickness distribution in the historical CMIP5 ensemble simulations and concluded that, while the basin-scale average sea ice thickness and trends in the Arctic is represented well within the observational uncertainty, spatial patterns of sea ice thickness are poorly simulated [59]. Specifically, the models fail to simulate the thickest ice near the coast of northern Greenland and the Canadian Arctic Archipelago and thinner ice over the Siberian Shelf. This is a critical bias, as the projected ice extent is strongly correlated to the initial ice thickness distribution [59]. It has been shown that ice thickness bias in the Siberian shelf seas is due to absence of the land-fast ice model in the

simulations [72,73]; most of the present-day climate models do not include fast ice physics. On the other hand, the MIZ dynamics is also poorly represented in the climate models [74], which historically use ice rheology developed for compact thick pack ice in the central Arctic [75]. The above and many other examples demonstrate importance of advanced, physically based sea ice models for the accurate predictions of Arctic sea ice evolution and decline. The ice thickness is a key parameter for assessing shipping routes navigability and time expenditures. Despite advances in the satellite technology, sea ice thickness observations are still difficult to make on the routine basis and during all seasons [59] and model reanalysis and predictions are still the main source of this vital information.

The simulations presented in this study project a 50 percent increase in the significant wave height H_w (Fig. 8). Both observations and the hindcast simulations already show an increase in H_w in the Arctic Ocean between the 1990s and 2010s, with the average H_w doubling in the Chukchi and Beaufort Seas [76]. Over this period extreme wave heights have also increased and their recurrence has more than doubled [76]. Thomson and Rogers present observations of H_w reaching over 5 metres in the Beaufort Sea in September 2012 [52]. This increase in H_w is attributed to the thinning of sea ice and a longer wave fetch [76]. Since most projections (including the present HaDGEM2 projection) also suggest a significant (50 percent or more) increase in the wind speed, a larger than 100 percent increase in H_w in the Arctic Ocean in the 21st century is probable [77]. Higher winds and waves, combined with subzero air temperature in the winter, may increase the danger of icing, which has accounted for a substantial number of ship accidents and shipwrecks on the NSR [78]. This poses significant challenges to navigation and offshore exploration, as well as for the ship classification and insurance industries.

Another key result from the simulation is a significant change in the Arctic Ocean circulation, at the surface as well as at depth. By the 2090s the cyclonic flow of the intermediate water in the Canada Basin becomes anti-cyclonic and the boundary current in the Canadian Basin and

the Laptev Sea reverses. The changes are similar to those discussed by Karcher and co-workers [79]. In their paper the changes in wind and reduction of sea ice cover were responsible for modification of the momentum transfer from atmosphere to the ocean, leading to an increased anti-cyclonicity in the ocean circulation and reversal of currents. Our forward simulation suggests a potentially complex picture of the future Arctic Ocean Change, highlighting the importance of high-resolution forecasts and challenging the views that most of the changes in the Arctic concern sea ice and the atmosphere.

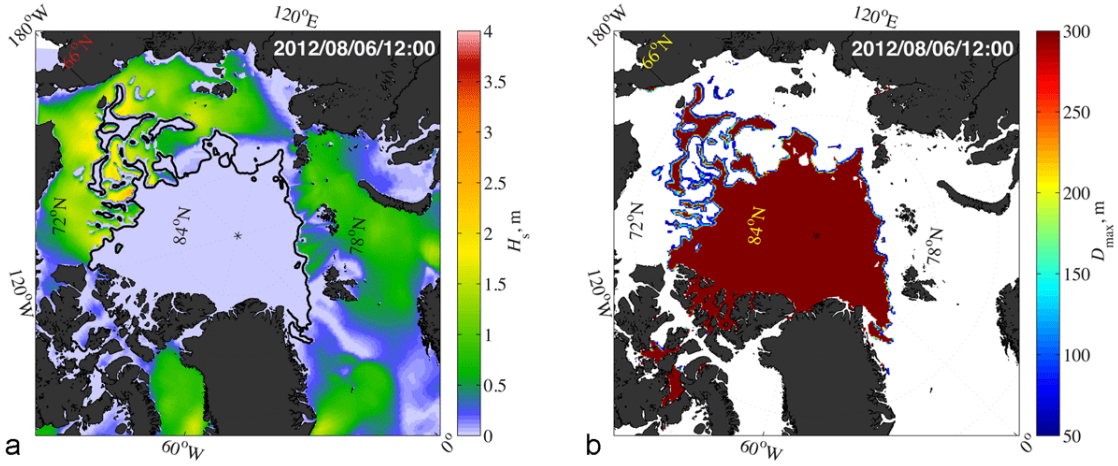

Fig. 9. Examples of Arctic wave and ice forecasts with the Towards an Operational Prediction system for the North Atlantic European coastal Zones (TOPAZ): (a) maximum significant wave heights (color) on 6 Aug 2012 12.00 GMT and (b) the same but for maximum floe size (http://topaz.nersc.no/).

The changes in the Arctic ocean surface and subsurface currents may potentially affect planning of maritime operations in several ways. Firstly, in the absence of sea ice, surface currents become one of the prime factors influencing ship safety, safe speed and sailing times. Secondly, they impact the redistribution of icebergs around Greenland and in the Canadian Arctic Archipelago. Due to a potential "short-circuiting" of the Arctic surface circulation in the Nordic Sea (Fig. 4) some Greenland icebergs may potentially reach Arctic shipping routes. Simulations with an iceberg model coupled to the NEMO OGCM [80] show iceberg spread in the central Arctic Ocean. Lastly, the environmental impact of potential shipping accidents or

pollution during the navigation will depend on ocean currents. The pathways can be addressed using high-resolution simulations to track pollutant spread by ocean currents and sea ice.

5. Conclusions and Policy Implications

According to the simulations, before the 2030s the principal factors for navigation and ship safety are the sea ice conditions. For long term planning, as well as for operational support of navigation and maritime industry, the present transport accessibility models which use static information such as sea ice concentration and sea ice types (e.g. ATAM) are adequate in the pack ice areas. However, the acceleration in sea ice drift that has occurred in the last decade requires accounting for sea ice dynamics, i.e., ice drift and ice internal pressure due to sea ice convergence and compression [81]. Marchenko analysed shipping accidents and shipwrecks on the NSR occurring between the 1930s and 1990s and concluded that ice drift and compression caused about a half of the shipwrecks [78,82], highlighting ice jets (a rapid sea ice flow between drifting and land-fast ice, typically generated by storm surges) as the most dangerous phenomenon for marine transportation in the area.

For more detailed short-term forecasting, a route optimization algorithm is needed to estimate sailing times and accessibility projections should be extended by developing a route optimization tool to estimate the fastest trans-Arctic route given the ice conditions for a particular season and year [26,83] Additional improvements of the optimal route simulations are envisaged since the present-day coupled atmosphere–ocean general circulation models are continue incorporating more advanced representation of sea ice, ocean and atmosphere physics, amongst these, ice ridging and thermal decay affect shipping the most [26].

After the 2030s, when pack ice begin to decline and MIZ-type sea ice provinces emerge, new approaches to forecasting should be considered. The new transport and accessibility models will require more information, including forecasts of winds, currents and waves. More

detailed sea ice data will also be required, such as sea ice floe sizes and ice drift parameters. Definitions of sea ice mechanical properties (used for example by oil-rig designers) may need revisiting, as sea ice would be thinner, more saline and weaker [84].

Presently, Arctic exploitation is the centre of discussion, weighing mitigation of consequences of the Arctic changes against potential economical benefits. Therefore there is a little surprise, that after a century of intensive Arctic exploration and more than a six decades of using Arctic shipping routes, the economical viability of Arctic shipping is still debated [85]. The challenges are great and lie in balancing economic drivers in Europe, the Americas and in the far-eastern countries, such as China, Malaysia, Singapore, Taiwan [86,87], economic risk [85] a need for Arctic infrastructure development, accessible modern ports, roads, etc. [88], and also the impact on the Arctic communities, ecosystems, as well as political and social drivers.

Another caveat is that, while the shift of shipping to shorter Arctic routes may decrease fuel use and lower CO_2 emissions, the impact on climate warming may not be wholly negative. This is because the use of Arctic routes may lead to increased concentrations of non-CO_2 gases, aerosols and particles in the Arctic, which can change radiative forcing (e.g. deposition of black carbon on sea ice and snow) and produce more complex regional warming/cooling effects. Simulations of these aspects of Arctic routes suggest that there may actually be a net global warming effect before net cooling takes over [89], thus suggesting that changes in the Arctic maritime use could potentially affect the global economy and global natural environment.

The changes in the Arctic natural environment are occurring faster than elsewhere in the world, and are likely to continue that way for the next few decades with an increased variability of the environmental parameters. They require a system-based approach, combining expertise in different areas, natural and social sciences, engineering, economics,

law, policymaking and ecology, capitalizing on the synergy between disciplines. This requires cross-subject international collaboration and close links between science, engineering and industry. For the shipping industry it is important to initiate cooperation with the forecasting, climate modeling, sea ice, oceanographic and atmospheric observational and modelling communities in order to establish requirements for the environmental data and forecasts [23]. This will help assessing the potential benefits and risks of Arctic maritime operations and make them safe.

The present study gives an overview of potential changes in the Arctic relevant to the operation of the sea routes and discusses approaches and challenges in modelling them. The study neither advocates the usage of the Arctic routes, nor presents a complete forecast of the Arctic conditions suitable for detailed shipping planning. For the former, it necessitates a comprehensive socio-economic analysis of Arctic navigation, which is beyond the scope of this study, whereas the latter requires further in-depth modelling studies addressing uncertainties in future projections. To the best of the authors' knowledge, this study presents one of the first attempts to combine comprehensive detailed high-resolution environmental information on the future state of sea ice and ocean in the Arctic for practical use by the shipping industry.

The study is linked to several oceanographic initiatives and projects and specifically co-operates with the EU FP7 SWARP Project on introducing ocean wave information and ice break up in the MIZ, as well as with UKMO Earth System Model (ESM) development. With this study the authors have attempted to demonstrate the need for closer interactions between environmental science, engineering and industry in a changing global environment and envisage strong benefits from creating these links.

Acknowledgements

The authors are grateful to Dr. Andrew Coward (NOC) for the help with the global NEMO-ROAM model configuration and Jean Bidlot (ECMWF) for providing the study with the WAM model data. The authors are also thankful to Prof Kay Riska (Total) for his illuminating talk on the present-day Arctic maritime operations, presented at the Sea Ice Royal Society Meeting in September 2014 and for his comments on the manuscript, to Dr Scott Stephenson (University of Connecticut, CT, USA) for his enthusiasm in discussing industrial and societal consequences of Arctic environmental change, and to Dr Michael Traut (University of Manchester, UK) for his lecture on the impact of the commercial shipping on Climate, given at the NOC in October 2014 and for the follow up conversations. The waves-in-ice simulation relied on the Norwegian Meteorological Institute (Met Norway) for initial conditions and the Institut français de recherché pour l'exploitation de la mer (Ifremer) for wave information over its duration. The manuscript was also inspired by discussions at the annual Forum for Arctic Modeling and Observing Synthesis (FAMOS) meetings. The authors are also grateful to the anonymous referees for the valuable comments and suggestions, which helped to improve the manuscript. The authors would like to thank the organisers of the Shipping in Changing Climate Conference, which took place in Liverpool in June 2014 under the umbrella of International Business Festival, for providing an excellent opportunity for interaction and discussions between scientists and industry.

Funding for the study

Drs. Aksenov, Bergh, Bertino, Nurser and Williams acknowledge support from European Union Seventh Framework Programme SWARP (grant agreement 607476) for this research. Drs. Aksenov, Nurser, Popova and Yool were also funded from the UK Natural Environment Research Council (NERC) Marine Centres' Strategic Research Programme. Dr. Aksenov also

was supported from the UK NERC TEA-COSI Research Project (NE/I028947/). The authors are thankful to FAMOS (funded by the National Science Foundation Office of Polar Programs, awards PLR-1313614 and PLR-1203720) for travel support to attend FAMOS meetings. The global simulation work in this study was performed as part of the Regional Ocean Acidification Modelling project (ROAM; NERC grant number NE/H01732/1) and part-funded by the European Union Seventh Framework Programme EURO-BASIN (FP7/2007-2013, ENV.2010.2.2.1-1; grant agreement 264933). The study used supercomputing facilities provided by the Norwegian Metacenter for Computational Science (Notur). The NEMO-ROAM025 simulations were performed on the ARCHER UK National Supercomputing Service (http://www.archer.ac.uk).

1 Glossary

AIRSS	Arctic Ice Regime Shipping System
AB	Arctic Bridge
AR	Assessment Reports
ATAM	Arctic Transport Accessibility Model
CAC	Canadian Arctic Categories
CICE	C-ICE Los Alamos sea ice model
CMIP5	Coupled Model Intercomparison Project 5
ECMWF	European Center for Medium Range Weather Forecasting
EEDI	Energy Efficiency Design Index
EU	European Union
EVP	Elastic-Viscous-Plastic Sea Ice rheology
FYI	First-year ice
GMES	Global Monitoring for Environment and Security
HadGEM2-ES	Hadley Center Global Environment Earth System Model, version 2
HadISST1	Hadley Centre Sea Ice and Sea Surface Temperature
IASC	International Association of Classification Societies
IM	Ice Multiplier
IMO	International Maritime Organisation
IN	Ice Numeral
INSROP	International Northern Sea Route Program
IPCC	Intergovernmental Panel on Climate Change
LIM2	Louvain-la-Neuve Sea Ice Model
LNG	Liquid Natural Gas
MYI	Multi-year ice
MIZ	Marginal Ice Zone
NEMO	Nucleus for European Modelling of the Ocean modeling framework
NPR	Arctic North Pole Route
NSR	Northern Sea Route
NWP	North-west Passage
OGCM	Ocean General Circulation Model
OPA	Ocean Parallelisé Model
PIOMAS	Pan-Arctic Ice-Ocean Modeling and Assimilation System reanalysis
RCP	Representative Concentration Pathways
ROAM	Regional Ocean Acidification Modelling
SS	Ship Safe Speed
ST	Sailing Time
SWARP	EU Project “Ships and Waves Reaching Polar Regions”
TOPAZ	Towards an Operational Prediction system for the North Atlantic European coastal Zones
UKMO	UK Meteorological Office
UNFCC	United Nations Framework Convention on Climate Change
WIM	Wave in Ice Model
WMO	World Meteorological Organisation

2

Appendix 1. Calculation of safe ship speed and sailing times

Following the Arctic Transport Accessibility Model (ATAM) of Stephenson et al. (2011b), the Ice Numerals (IN) are given by (1):

$$IN = A_{Ni}\times IM_{Ni} + A_{G}\times IM_{G} + A_{Gw}\times IM_{Gw} + A_{FY1}\times IM_{FY1} + A_{FY2}\times IM_{FY2} +$$

$$+A_{MFY}\times IM_{MFY} + A_{TFY}\times IM_{TFY} + A_{SY}\times IM_{SY} + A_{MY}\times IM_{MY} \quad (1),$$

where $A_{Ni,G,GW,\ldots,MY}$ and $IM_{Ni,G,GW,\ldots,MY}$ is the sea ice concentration for different Ice Types (IT) and corresponding Ice Multipliers (IM) (Table 1). Ice Types are derived from the mean sea ice thickness in the model cell (Table 1), as it is a good representation of the ice stage of ice development (ice age), (e.g., Maskanik et al, 2007). From the Ice Numerals, the safe ship speed (SS) is defined for each grid cell on a shipping route (Table 2). The sailing time (ST) is defined by adding the time required to cross all model cells along the route (2).

$$ST = \sum_{i=1}^{N} {}^{D_i}/_{SS_i} \quad (2).$$

Here D_i and SS_i are the distances across- and ship safe speed for- each model cell. D_i is calculated as a half of the distance between the central points of two model cells along the chosen sailing track, and there are a total of *N* model cells along the sailing track.

Appendix 2. Maximum floe sizes

Maximum sea ice floe size can be empirically related to sea ice concentration as follows (Lüpkes et al., 2012):

$$L_i = L_{min}\left(1 - {}^{A_*}/_{A}\right)^{\beta} \quad (3).$$

Here $L_{\min}$ - is the minimum flow size, β is an exponent to fit the observational the data (here $\beta = 1$), and A and A^* – are the actual and maximum sea ice concentration, where the latter can be written as below:

$$A_* = (1 - L_{min}/L_{max})^{-1/\beta} \quad (4).$$

Tables

Table 1. Ice Multipliers (IM) for different Ice Types and Ship Classes (Arctic Ice Regime Shipping System, 1998). Details are in the text

WMO Ice Type	WMO Ice Thickness (m)	Ship Classes						
		Type E (OW)	Type D	Type C	Type B	Type A (PC6)	CAC4	CAC3 (PC3)
MY	300-400*	-4	-4	-4	-4	-4	-3	-1
SY	250-300*	-4	-4	-4	-4	-3	-2	1
TFY	120-250*	-3	-3	-3	-2	-1	1	2
MFY	70-120	-2	-2	-2	-1	1	2	2
FY 2	50-70	-1	-1	-1	1	2	2	2
FY 1	30-50	-1	-1	1	1	2	2	2
GW	15-30	-1	1	1	1	2	2	2
G	10-15	1	2	2	2	2	2	2
Ni	<10	2	2	2	2	2	2	2

Table 2. Ship safe speed (SS) in nautical miles per hour (nm/h) by Ice Numeral (IN) (Table 1) following AIRSS (Arctic Ice Regime Shipping System, 1998) and Stephenson et al. (2011a,b)

Ice Numeral	Safe speed (nm/h)
<0	0 (Impassable/not safe)
0-8	4
9-13	5
14-15	6
16	7
17	8
18	9
19	10
20	11

Table 3. Predicted averaged sailing time (ST) in days for different Ship Classes (Arctic Ice Regime Shipping System, 1998) along the NPR for the summers 2010-2019 and 2030-2039; n/s - marks sailing is not safe; number in brackets show sailing time for the routes optimised to avoid impassible ice type for different ship classes (Table 1).

Ship Class	NPR ST 2010-2019 (days)	NPR ST 2030-2039 (days)
CAC3 (PC3)	n/s (16)	13
CAC4	n/s (19)	13
Type A (PC6)	n/s (20)	15
Type B	n/s (20)	16
Type C	n/s (21)	n/s (16)
Type D	n/s (21)	n/s (17)
Type E (OW)	n/s (21)	n/s (17)
Range	(16- 21)	13-16(17)

References

[1] Heitmann N, Khalilian S. Accounting for carbon dioxide emissions from international shipping: burden sharing under different UNFCCC allocation options and regime scenarios. Mar. Policy 2011; 35(5): 682–691.

[2] Anderson K, Bows A. Beyond 'dangerous' climate change: emission scenarios for a new world. Phil Trans R Soc A: Math Phys Eng Sci 2011; 369: 20-44.

[3] Anderson K, Bows A. Executing a Scharnow turn: reconciling shipping emissions with international commitments on climate change. Carbon Manage 2012; 3(6): 615–28.

[4] Bows-Larkin A, Anderson K, Mander S, Traut M, Walsh C. Shipping charts a high carbon course. Nature Climate Change 2015; 5: 293-95.

[5] Bazari Z, Longva T. Assessment of IMO mandated energy efficiency measures for international shipping. Estimated CO_2 emissions reduction form introduction of mandatory technical and operational energy efficiency measures for ships. Project Final Report, MEPC 63/INF.2, October 31, 2011.

[6] International Maritime Organization. Reduction of GHG emissions from ships. Third IMO GHG Study 2014 - Executive Summary and Final Report. MEPC 67/INF.3, June 2014.

[7] Traut M, et al. Propulsive power contribution of a kite and a Flettner rotor on selected shipping routes. Applied Energy 2014; 113: 362-72.

[8] Eide MS, Longva T, Hoffmann P, Endresen Ø, Dalsøren SB. Future cost scenarios for reduction of ship CO_2 emissions. Maritime Policy and Management 2011; 38(1): 11-37, DOI: 10.1080/03088839.2010.533711.

[9] Eide MS, Endresen Ø, Skjong R, Longva T, Alvik S. Cost-effectiveness assessment of CO_2 reducing measures in shipping. Maritime Policy and Management 2009; 36(4): 367-84, DOI: 10.1080/03088830903057031.

[10] Schøyen H, Bråthen S. The Northern Sea Route versus the Suez Canal: cases from bulk shipping. J Transport Geography 2011; 19(4): 977-83.

[11] Liu M, Kronbak J. The potential economic viability of using the Northern Sea Route (NSR) as an alternative route between Asia and Europe. J Transport Geography 2010; 18(3): 434-44.

[12] Stephenson SR., Smith LC, Agnew JA. Divergent long-term trajectories of human access to the Arctic. Nature Climate Change 2011; 1: 156-60, DOI: 10.10-38/NCLIMATE1120.

[13] Farré AB, Stephenson SR, Chen L, Czub M, Dai Y, Demchev D, Efimov Y, et al. Commercial Arctic shipping through the Northeast Passage: routes, resources, governance, technology, and infrastructure. Polar Geography 2014; 37(4): 298-324, DOI: 10.1080/1088937X.2014.965769.

[14] Brubaker RD, Ragner CL. A review of the International Northern Sea Route Program (INSROP) - 10 years on. Polar Geography 2010; 33(1-2): 15-38, DOI: 10.1080/1088937X.2010.493308.

[15] Andersen Ø, Heggeli TJ, Wergeland T. III.10.1: Assessment of Potential Cargo from and to Europe via the NSR. INSROP Working Paper 11-1995. Lysaker: INSROP Secretariat; 1995.

[16] Tamvakis M, Granberg A, Gold E. Economy and commercial viability. In: Ostreng W, editor. The Natural and Societal Challenges of the Northern Sea Route: A Reference Work. Dordrecht/Boston/London: Kluwer Academic Publishers; 1999.

[17] Ragner CL. Northern Sea Route Cargo Flows and Infrastructure – Present State and Future Potential. FNI Report 13/2000. Lysaker: Fridtjof Nansen Institute; 2000.

[18] Ragner CL. The Northern Sea Route - Commercial Potential, Economic Significance, and Infrastructure Requirements. Post-Soviet Geography and Economics 2000; 41(8): 541-80. Available at: <http://dx.doi.org/10.1080/10889388.2000.10641157>.

[19] Mitchell T, Milne R. Chinese cargo ship sets sail for Arctic short-cut. Financial Times, August 11, 2013. Available at: <http://www.ft.com>.

[20] Brigham LW, Ellis B, editors. Arctic marine transport workshop (Scott Polar Research Institute, University of Cambridge, 28–30 September 2004). Institute of the North, US Arctic Research Commission, International Arctic Science Committee. Anchorage (AK): Northern Printing; 2004.

[21] Stephenson SR, Brigham LW, Smith LC. Marine accessibility along Russia's Northern Sea Route. Polar Geography 2014; 37(2): 111-33, doi:10.1080/1088937X.2013.845859.

[22] North Sea Route Information Office. 2015. Available at: <http://www.arctic-lio.com/nsr_transits>.

[23] Rogers TS, et al. Future Arctic marine access: analysis and evaluation of observations, models, and projections of sea ice. The Cryosphere 2013; 7: 321-32.

[24] Flato G, Marotzke J, Abiodun B, Braconnot P, Chou SC, Collins W, Cox P, Driouech F, Emori S, Eyring V, Forest C, Gleckler P, Guilyardi E, Jakob C, Kattsov V, Reason C, Rummukainen M. Evaluation of Climate Models. In: Stocker TF, Qin D, Plattner GK, Tignor M, Allen SK, Boschung J, Nauels A, Xia Y, Bex V, Midgley PM, editors. Climate Change 2013: The Physical Science Basis. Contribution of Working Group I to the Fifth Assessment Report of the Intergovernmental Panel on Climate Change. Cambridge (UK) and New York (NY): Cambridge University Press; 2013.

[25] Vaughan DG, et al. Observations: Cryosphere. In: Stocker TF, Qin D, Plattner GK, Tignor M, Allen SK, Boschung J, Nauels A, Xia Y, Bex V, Midgley PM, editors. Climate Change 2013: The Physical Science Basis. Contribution of Working Group I to the Fifth Assessment Report of the Intergovernmental Panel on Climate Change. Cambridge (UK) and New York (NY): Cambridge University Press; 2013.

[26] Smith LC, Stephenson SR. New Trans-Arctic shipping routes navigable by midcentury. Proceedings of the National Academy of Sciences 2013; 110(13): E1191-E1195.

[27] Stephenson SR, Smith LC, Brigham LW, Agnew JA. Projected 21st-century changes to Arctic marine access. Climatic Change 2013; 118(3-4): 885-99.

[28] Riska K. Impacts on Navigation of Arctic Sea Ice Change. Proceedings of Royal Society (in review) 2014.

[29] Nurser AJG, Bacon S. Eddy length scales and the Rossby radius in the Arctic Ocean. Ocean Sci Discuss 2013; 10(5): 1807-31.

[30] Yool A, Popova EE, Coward AC, Bernie D, Anderson TR. Climate change and ocean acidification impacts on lower trophic levels and the export of organic carbon to the deep ocean. Biogeosciences 2013; 10: 5831-54.

[31] Madec G and NEMO team. NEMO ocean engine, version 3.4. Note du Pole de modelisation de l'Institut Pierre-Simon Laplace, No 27 ISSN No 1288-1619; 2012.

[32] Fichefet T, Maqueda MÁM. Sensitivity of a global sea ice model to the treatment of ice thermodynamics and dynamics. J Geophys Res: Oceans (1978–2012) 1997; 102(C6): 12609-46.

[33] Bouillon S, Maqueda MÁM, Legat V, Fichefet T. An elastic–viscous–plastic sea ice model formulated on Arakawa B and C grids. Ocean Modelling 2009; 27(3): 174-84.

[34] Storkey D, Blockley EW, Furner R, Guiavarc'h C, Lea D, Martin MJ, Barciela RM, Hines A, Hyder P, Siddorn JR. Forecasting the ocean state using NEMO: The new FOAM system. J Operational Oceanography 2010; 3(1): 3-15.

[35] Dufresne J-L, Foujols M-A, Denvil S, Caubel A, Marti O, Aumont O, Balkanski Y, et al. Climate change projections using the IPSL-CM5 Earth System Model: from CMIP3 to CMIP5. Climate Dynamics 2013; 40(9-10): 2123-65.

[36] Rogelj J, Meinshausen M, Knutti R. Global warming under old and new scenarios using IPCC climate sensitivity range estimates. Nature Climate Change 2012; 2: 248-53, DOI:10.1038/NCLIMATE1385.

[37] Collins M, et al. Long-term Climate Change: Projections, Commitments and Irreversibility. In: Stocker TF, Qin D, Plattner GK, Tignor M, Allen SK, Boschung J, Nauels A, Xia Y, Bex V, Midgley PM, editors. Climate Change 2013: The Physical Science Basis. Contribution of Working Group I to the Fifth Assessment Report of the Intergovernmental Panel on Climate Change. Cambridge (UK) and New York (NY): Cambridge University Press; 2013.

[38] Jones, CD, et al. The HadGEM2-ES implementation of CMIP5 centennial simulations. Geosci Model Dev 2011; 4: 543–70, DOI:10.5194/gmd-4-543-2011.

[39] Large WG, Yeager SG. The global climatology of an interannually varying air-sea flux data set. Climate Dynamics 2009; 33(2-3): 341–64, DOI:10.1007/s00382-008-0441-3.

[40] Friedlingstein P, et al. Persistent growth of CO_2 emissions and implications for reaching climate targets. Nature Geoscience 2014; 7: 709-15.

[41] Peters GP, et al. The challenge to keep global warming below 2C. Nature Climate Change 2013; 3: 4-6.

[42] Popova EE, Yool A, Aksenov Y, Coward AC, Anderson TR. Regional variability of acidification in the Arctic: a sea of contrasts. Biogeosciences 2014; 11: 293-308.

[43] Aksenov Y, Ivanov VV, Nurser AJG, Bacon S, Polyakov IV, Coward AC, Naveira-Garabato AC, Beszczynska-Moeller A. The Arctic circumpolar boundary current. J Geophys Res: Oceans (1978–2012) 2011; 116(C09017).

[44] Stephenson SR, Smith LC, Agnew JA. Divergent long-term trajectories of human access to the Arctic. Supplementary Information Nature Climate Change 2011; 1(3): 1-28, DOI: 10.10-38/NCLIMATE1120.

[45] Arctic Ice Regime Shipping System (AIRSS) Standards. Ottawa: Transport Canada; 1998.

[46] World Meteorological Organization. WMO sea-ice nomenclature: Terminology, codes and illustrated glossary. (WMO/OMM/ BMO 259, TP 145, revision Mar 2010). Geneva: World Meteorological Organization; 1970.

[47] Flocco D, Schroeder D, Feltham DL, Hunke EC. Impact of melt ponds on Arctic sea ice simulations from 1990 to 2007. J Geophys Res: Oceans (1978–2012) 2012; 117(C9).

[48] Timco G, Johnston M. Arctic Ice Regime Shipping System Pictorial Guide - TP14044. January 2003. Ottawa: Canadian Hydraulics Institute, Transport Canada; 2003.

[49] International Association of Classification Societies (IACS) Unified Requirements for Polar Class Ships. Ottawa: Transport Canada; 2009.

[50] Strong C, Rigor IG. Arctic marginal ice zone trending wider in summer and narrower in winter. Geophys Res Lett 2013; 40(18): 4864-68.

[51] Lüpkes C, Gryanik VM, Hartmann J, Andreas EL. A parametrization, based on sea ice morphology, of the neutral atmospheric drag coefficients for weather prediction and climate models. J Geophys Res: Atmospheres (1984–2012) 2012; 117(D13).

[52] Thomson J, Rogers WE. Swell and sea in the emerging Arctic Ocean. Geophys Res Lett 2014; 41(9): 3136-40.

[53] Williams TD, Bennetts LG, Squire VA, Dumont D, Bertino L. Wave–ice interactions in the marginal ice zone. Part 1: Theoretical foundations. Ocean Model 2013; 71: 81-91.

[54] Rayner NA, Parker DE, Horton EB, Folland CK, Alexander LV, Rowell DP, Kent EC, Kaplan A. Global analyses of sea surface temperature, sea ice, and night marine air temperature since the late nineteenth century. J Geophys Res: Oceans 2003; 108(D14): 4407, DOI:10.1029/2002JD002670.

[55] Zhang J, Thomas DR, Rothrock DA, Lindsay RW, Yu Y, Kwok R. Assimilation of ice motion observations and comparisons with submarine ice thickness data. J Geophys Res: Oceans 2003; 108(C6): 3170, doi:10.1029/2001JC001041.

[56] Overland JE, Wang M. When will the summer Arctic be nearly sea ice free? Geophys Res Lett 2013, 40: 2097–2101, DOI:10.1002/grl.50316.

[57] Stroeve JC, Kattsov V, Barrett A, Serreze M, Pavlova T, Holland M, Meier WN. Trends in Arctic sea ice extent from CMIP5, CMIP3 and observations. Geophys Res Lett 2012; 39(L16502), DOI:10.1029/2012GL052676.

[58] Malone ED, et al. North American Climate in CMIP5 Experiments: Part III: Assessment of Twenty-First-Century Projections. J Climate 2014; 27(6): 2230–70. Available at: <http://dx.doi.org/10.1175/JCLI-D-13-00273.1>.

[59] Stroeve JC, Barrett A, Serreze M, Schweiger A. Using records from submarine, aircraft and satellites to evaluate climate model simulations of Arctic sea ice thickness. The Cryosphere 2014; 8: 1839-54. [52] Thomson J, Rogers WE. Swell and sea in the emerging Arctic Ocean. Geophys Res Lett 2014; 41(9): 3136-40.

[60] Hezel PJ, Fichefet T, Massonnet F. Modeled Arctic sea ice evolution through 2300 in CMIP5 extended RCPs. The Cryosphere 2014; 8(4): 1195-1204.

[61] Comiso JC, Nishio F. Trends in the sea ice cover using enhanced and compatible AMSR-E, SSM/I, and SMMR data. J Geophys Res 2008; 113(C02S07), DOI:10.1029/2007JC004257.

[62] Giles KA, Laxon S, Ridout AL, Wingham DJ, Bacon S. Western Arctic Ocean freshwater storage increased by wind driven spin-up of the Beaufort Gyre. Nature Geoscience 2012; 5: 194-97, DOI: 10.1038/NGEO1379.

[63] Farrell SL, McAdoo DC, Laxon SW, Zwally HJ, Yi D, Ridout A, Giles K. Mean dynamic topography of the Arctic Ocean. Geophys Res Lett 2012; 39(L01601).

[64] Proshutinsky A, Krishfield R, Timmermans ML, Toole J, Carmack E, McLaughlin F, Williams WJ, Zimmermann S, Itoh M, Shimada K. Beaufort Gyre freshwater reservoir: State and variability from observations. J Geophys Res 2009; 114(C00A10), DOI:10.1029/2008JC005104.

[65] Sakov P, Counillon F, Bertino L, Lisæter KA, Oke PR, Korablev A. TOPAZ4: an ocean-sea ice data assimilation system for the North Atlantic and Arctic. Ocean Sci 2012; 8: 633-56.

[66] Dumont D, Kohout A, Bertino L. A wave-based model for the marginal ice zone including a floe breaking parameterization. J Geophys Res 2011; 116(C04001): 1–12, DOI:10.1029/2010JC006682.

[67] Squire VA, Williams TD, Bennetts LG. Better operational forecasting for contemporary Arctic via ocean wave integration. International Journal of Offshore Polar Engineering 2013: 23(2): 81-88.

[68] Jeffries MO, Overland JE, Perovich DK. The Arctic shifts to a new normal. Physics Today 2013; 66(10): 35, DOI: 10.1063/PT.3.2147.

[69] Overland JE, Wang M, Walsh JE, Stroeve JC. Future Arctic climate changes: Adaptation and mitigation time scales. Earth's Future 2013b; 2(2): 68-74, DOI:10.1002/2013EF000162.

[70] Koenigk T, Brodeau , Graversen RG, Karlsson J, Svensson G, Tjernström M, Willén U, Wyser K. Arctic climate change in 21st century CMIP5 simulations with EC-Earth. Climate dynamics 2013; 40(11-12: 2719-43.

[71] Stroeve JC, Markus T, Boisvert L, Miller L, Barrett A. Changes in Arctic melt season and implications for sea ice loss, Geophys Res Lett 2014b; 41: 1216–25, doi:10.1002/2013GL058951

[72] Johnson M, Proshutinsky A, Aksenov Y, Nguyen AT, Lindsay R, Haas C, ... & Cuevas B. Evaluation of Arctic sea ice thickness simulated by Arctic Ocean Model Intercomparison Project models 2012: Journal of Geophysical Research: Oceans: 117(C8).

[73] Janout M, Aksenov Y, Hölemann J, Rabe B, Schauer U, Polyakov I, Bacon S, Coward A, Karcher M, Lenn YD, Kassens H, Timokhov L. Kara Sea freshwater transport through Vilkitsky Strait: Variability, forcing, and further pathways from a model and observations 2015: Journal of Geophysical Research: Oceans: accepted.

[74] Zhang J., Schweiger A, Steele M, Stern H. Sea ice floe size distribution in the marginal ice zone: Theory and numerical experiments 2015; J. Geophys. Res. Oceans: 120, doi:10.1002/2015JC010770.

[75] Feltham DL. Granular flow in the marginal ice zone. Philosophical Transactions of the Royal Society of London A: Mathematical, Physical and Engineering Sciences 2005; 363(1832): 1677-1700.

[76] Francis OP, Panteleev GG, Atkinson DE. Ocean wave conditions in the Chukchi Sea from satellite and in situ observations. Geophys Res Lett 2011; 38(L24610).

[77] Khon VC, Mokhov II, Pogarskiy FA, Babanin A, Dethloff K, Rinke A, Matthes H. Wave heights in the 21st century Arctic Ocean simulated with a regional climate model. Geophys Res Lett 2014; 41(8): 2956–61, DOI:10.1002/2014GL05984.

[78] Marchenko NA. Russian Arctic Seas. Navigation conditions and accidents: Springer; 2012: 278 pp.

[79] Karcher M, Smith JN, Kauker F, Gerdes R, Smethie Jr WM. Recent changes in Arctic Ocean circulation revealed by iodine-129 observations and modeling. J Geophys Res 2012; 117(C08007), DOI:10.1029/2011JC007513.

[80] Marsh R, Ivchenko VO, Skliris N, Alderson S, Bigg GR, Madec G, Blaker A, Aksenov Y. NEMO-ICB (v1.0): interactive icebergs in the NEMO ocean model globally configured at eddy-permitting resolution. Geosci Model Dev 2015; 8(5): 1547-62, DOI:10.5194/gmdd-7-5661-2014.

[81] Somanathan S, Flynn P, Szymanski J. The Northwest Passage: A simulation. Transportation Research Part A: Policy and Practice 2009; 43(2): 127-35.

[82] Marchenko NA. Navigation in the Russian Arctic. Sea Ice caused Difficulties and Accidents. Offshore and Arctic Engineering 2013; 32nd International Conference on Ocean OMAE 2013, June, France. OMAE2013-10546.

[83] Kotovirta V, Jalonen R, Axell L, Riska K, Berglund R. A system for route optimization in ice-covered waters. Cold Regions Science and Technology 2009; 55(1): 52-62.

[84] Sanderson TJO. Ice mechanics and risks to offshore structures. Norwell (MA): Kluwer Academic Publishers; 1988.

[85] Lasserre F. Case studies of shipping along Arctic routes. Analysis and profitability perspectives for the container sector. Transportation Research Part A: Policy and Practice 2014; 66: 144-161.

[86] Ho J. The implications of Arctic sea ice decline on shipping. Marine Policy 2010; 34(3): 713-715.

[87] Hong N. The melting arctic and its impact on china's maritime transport. Research in transportation economics 2012; 35(1): 50-57.

[88] Noble B, Ketilson S, Aitken A, Poelzer G. Strategic environmental assessment opportunities and risks for Arctic offshore energy planning and development. Marine Policy 2013; 39: 296-302.

[89] Fuglestvedt JS, et al. Climate Penalty for Shifting Shipping to the Arctic. Environ Sci Technol 2014; 48(22): 13273-79.

1 List of Figures

2 Fig. 1. (a) Region of the study. (b) Timeseries of the global annual mean surface air
3 temperature 1860-2099 in the RCP2.6 and RCP8.5 projected atmospheric forcing and (c)
4 of the pan-Arctic annual mean surface air temperature 2000-2099 in the RCP8.5 forcing.

5 Fig. 2. (a,c,e) Mean 1978-2005 winter (Dec–Feb) and (b,d,f) summer (Jun–Aug) sea ice
6 fraction (color and black contours) from the HadISST1 (Rayner et al., 2003) (a, b) and
7 from the NEMO-ROAM025 model (c, d). (e) Model winter (Dec–Feb) and (f) summer
8 (Jun–Aug) 2030–2039 ice fraction from the NEMO-ROAM025 RCP8.5 projection (color
9 and black contours).

10 Fig. 3. (a) winter (February) and (b) summer (September) observed sea ice extent 1953–2015
11 (green line) from NSIDC (Comiso and Nishio, 2008) and HadISST (Rayner et al, 2003)
12 datasets and simulated 1953–2099 in NEMO-ROAM025 RCP8.5 (magenta), NEMO-
13 ROAM1 RCP8.5 (yellow) and in NEMO-ROAM1 RCP2.6 simulations (light blue). Red
14 arrows show the start of the NEMO-ROAM025 run in 1978 and the end of the historical
15 forcing and beginning of the projected RCP8/5/2.6 forcing in 2005. (c). Monthly ice
16 volume simulated by NEMO-ROAM025 RCP8.5 (red) and from PIOMAS (blue) for
17 1980-2015. (d) The corresponding modelled seasonal cycle of ice volume (red) and from
18 PIOMAS (blue). Modelled seasonal volumes are also shown for 2030-2059 (green) and
19 2060-2099 (yellow). The insert shows the corresponding seasonal cycles of modeled
20 mean ice thicknesses. Solid lines mark means and color shading denotes ±one standard
21 deviation. (e) Winter (February) and (f) summer (September) sea ice extent anomaly
22 (relative to the 1986-2005 winter and summer means respectively) in the NEMO-
23 ROAM025 RCP8.5 simulations (magenta) and in the NEMO-ROAM1 simulations forced
24 by RCP8.5 (yellow) and RCP2.6 (light blue). The corresponding sea ice extent anomalies

in the CMIP5 ensembles for the different emission scenarios from the IPCCA report (Collins et al., 2013) are shown as solid color lines with shading denoting 5 to 95 percent of the ensembles. Green lines depict the observed winter and summer sea ice extent anomalies 1953-2015 obtained from NSIDC and HadISST datasets.

Fig. 4. Model mean sea surface heights (a) in 2040-2049 and (b) change between 2000–2009 and 2090–2099 from RCP8.5 NEMO projection. Mean 2040–2049 (c) and 2090–2099 (d) Montgomery potential (equivalent of geostrophic streamfunctions) at the 27.8 kg/m^3 density surface (about 300-600 m depth) from the same projection.

Fig. 5. Model 2010–2019 (a) and 2030–2039 (b) sea ice concentration (percent, color) and thickness (red contours) during the navigation period (Jun-Oct) from the RCP8.5 NEMO projection. The Arctic shipping routes are shown schematically: the Northern Sea Route (NSR) (yellow line), the North Pole Route (NPR) (green line) and the Northwest Passage (NWP) and Arctic Bridge (AB) (white line).

Fig. 6. (a) Mean 1978-2005 summer (Jun–Aug) sea ice fraction (color) and mean floe sizes in metres (black contours with pink labels). Ice fraction is from the Hadley Centre dataset (Rayner et al, 2003). Red and yellow lines mark the outer (ice fraction of 0.15) and inner (ice fraction of 0.80) boundaries of the MIZ (Strong and Rigor, 2013). (b) The same but for 2030–2039 from the NEMO projection. (c) Timeseries 1979–2011 of MIZ width in summer (J–S, red) and winter (F–A, blue) from Strong and Rigor (2013); insert shows the MIZ expansion between Aug 1983 and Aug 2010.

Fig. 7. (a) Ensemble mean winter 2080–2099 ice concentration (percent) in the CMIP5 models with the RCP8.5 forcing (adapted from Collins et al., 2013) and (b) in the NEMO-ROAM025 projection. Please note different colour scales. Magenta line in shows observed 15 percent concentration. (c) Mean 2000–2009 winter sea ice fraction (color)

from the HadISST1 (Rayner et al, 2003). (d) Is the same as (b) but in different colour scale for comparison. Red and yellow lines in (c,d) mark the outer and inner MIZ boundaries. Monthly mean (solid) relative area (percent) of MIZ (sea ice concentration between 15 and 80 percent) (e) and (f) of pack ice (sea ice concentration greater than 80 percent) in winter and summer from the NEMO-ROAM025 projection. The shading denotes ± one standard deviation and dashed lines depict fitted linear trends.

Fig. 8. (a) Mean 2000–2009 10-m height mean wind speed over the ocean and (b) corresponding wind speed change between 2000–2009 and 2090–2099 from the RCP8.5 forcing. (c) Mean 2000–2009 winter (Dec–Feb) significant wave heights (color) from the ECMWF wave model WAM (courtesy Jean Bidlot, ECMWF). (d) Mean 2090–2099 winter (Dec–Feb) significant wave height increase in percent (color and contours) estimated from 10-m height wind speed change between 2000-2009 and 2090-2099 in the RCP8.5 projection.

Fig. 9. Examples of Arctic wave and ice forecasts with the Towards an Operational Prediction system for the North Atlantic European coastal Zones (TOPAZ): (a) maximum significant wave heights (color) on 6 Aug 2012 12.00 GMT and (b) the same but for maximum floe size (http://topaz.nersc.no/).